OXFORD

Human Molecular Genetics, 2015, Vol. 24, No. 12 3372–3389

doi: 10.1093/hmg/ddv086
Advance Access Publication Date: 5 March 2015
Original Article

ORIGINAL ARTICLE

Combined gene/cell therapies provide long-term and pervasive rescue of multiple pathological symptoms in a murine model of globoid cell leukodystrophy

Alessandra Ricca[1,†], Nicole Rufo[1,†], Silvia Ungari[1], Francesco Morena[2], Sabata Martino[2], Wilem Kulik[3], Valeria Alberizzi[4], Alessandra Bolino[4], Francesca Bianchi[4], Ubaldo Del Carro[4], Alessandra Biffi[1] and Angela Gritti[1,*]

[1]San Raffaele Scientific Institute, Division of Regenerative Medicine, Stem Cells and Gene Therapy, San Raffaele Telethon Institute for Gene Therapy (TIGET), Via Olgettina 58, Milano 20132, Italy, [2]Department of Chemistry, Biology and Biotechnologies, University of Perugia, via del Giochetto, Perugia, Italy, [3]Laboratory of Genetic Metabolic Diseases, Academic Medical Center AMC, University of Amsterdam, Meibergdreef 9, Amsterdam, The Netherlands and [4]Division of Neuroscience, San Raffaele Scientific Institute, INSPE, Via Olgettina 58, Milano, Italy

*To whom correspondence should be addressed. Email: gritti.angela@hsr.it

Abstract

Globoid cell leukodystrophy (GLD) is a lysosomal storage disease caused by deficient activity of β-galactocerebrosidase (GALC). The infantile forms manifest with rapid and progressive central and peripheral demyelination, which represent a major hurdle for any treatment approach. We demonstrate here that neonatal lentiviral vector-mediated intracerebral gene therapy (IC GT) or transplantation of GALC-overexpressing neural stem cells (NSC) synergize with bone marrow transplant (BMT) providing dramatic extension of lifespan and global clinical–pathological rescue in a relevant GLD murine model. We show that timely and long-lasting delivery of functional GALC in affected tissues ensured by the exclusive complementary mode of action of the treatments underlies the outstanding benefit. In particular, the contribution of neural stem cell transplantation and IC GT during the early asymptomatic stage of the disease is instrumental to enhance long-term advantage upon BMT. We clarify the input of central nervous system, peripheral nervous system and periphery to the disease, and the relative contribution of treatments to the final therapeutic outcome, with important implications for treatment strategies to be tried in human patients. This study gives proof-of-concept of efficacy, tolerability and clinical relevance of the combined gene/cell therapies proposed here, which may constitute a feasible and effective therapeutic opportunity for children affected by GLD.

Introduction

Globoid cell leukodystrophy (GLD) is a lysosomal storage disease caused by deficient activity of β-galactocerebrosidase (GALC). GALC deficiency results in accumulation of galactosylceramide and its toxic derivative Psychosine (Psy) in myelinating cells, and to a minor extent, in neurons of both central nervous system (CNS) and peripheral nervous system (PNS), causing white matter deterioration and neurodegeneration. In the classic early

† These authors contributed equally.

Received: February 2, 2015. **Revised and Accepted:** March 4, 2015

infantile form children present with symptoms by the first 6 months of life, then rapidly lose their motor and cognitive skills and die within a few years (1).

Treatment attempts in GLD murine models include substrate reduction therapy (SRT) (2) and, largely, enzyme replacement strategies based on delivery of the recombinant protein (ERT) (3), systemic/intracerebral injection of adeno-associated vectors (AAV) or lentiviral vectors (LV) expressing a functional enzyme (4,5), transplantation of hematopoietic (6–11), neural (12,13) or mesenchymal stem cells (14–16). All these treatments provided variable metabolic correction and pathological amelioration but were overall modestly effective in counteracting disease progression, failing to address the global disease.

Allogeneic HSCT has reached clinical application for several LSDs, including GLD (17). The efficacy of HSCT depends on the rate of disease progression and extent of CNS involvement (18,19), leading to greater benefit if performed in the asymptomatic stage (20). The disproportion between a likely slow pace of microglial/macrophage cell replacement and enzymatic activity reconstitution in the affected nervous tissue and the rapidity of disease progression of early onset forms may account for the suboptimal efficacy of HSCT in GLD infants, who eventually develop progressive neurological and motor deterioration (21).

Several efforts have been put in developing combined approaches that could treat the global phenotype (CNS, PNS and periphery) of GLD murine models. Most of them included bone marrow transplant (BMT) that was coupled to SRT (22), systemic/intrathecal ERT (23), intracerebral/intrathecal injection of AAV vectors (24,25) or systemic injection of LV (26). These studies showed a variable extent of additivity or synergy of the treatments but at closer examination many results remain unclear. In particular, the overall suboptimal outcome of BMT, which ranged from moderately beneficial (24,26) to ineffective (27), hampered a clear assessment of its contribution in contrasting disease manifestations. Furthermore, massive AAV-mediated gene delivery achieved with multiple injections and different delivery routes was required either alone (28) or in combination with BMT (25) to ensure significant benefits, challenging the safety profile and the overall feasibility.

In the present study, we optimized combinatorial gene/cell therapy strategies that could achieve a 3-fold purpose: first, to efficiently target multiple sites of pathology within a suitable temporal opportunity; second, to be well tolerated; third, to be applicable in view of clinical translation. We exploited the robust LV-based GT platform to directly transfer a functional *galc* gene in CNS tissues (single intracerebral injection) or to achieve supraphysiological GALC activity in neural stem cells (NSCs), and the complementary biological features of neural and BM-derived cells to provide timely and long-lasting enzymatic rescue of multiple affected organs/tissues. We report that neural stem cell transplantation (NSCT) or LV-mediated intracerebral gene therapy (IC GT) performed in asymptomatic GLD mice synergize with BMT providing remarkable therapeutic benefit as compared with each single treatment, with dramatic extension of lifespan and global rescue of the GLD phenotype. Importantly, the favourable safety profile of each single treatment (5,11,29) was maintained in the combined setting. We then systematically and comprehensively addressed the nature of the different disease-associated pathological features, their progression and the extent to which they can be reversed, clarifying the relative contribution of treatments to the therapeutic outcome as well as the relative contribution of CNS, PNS and periphery to the disease, with implications for treatment strategies to be tried in human patients.

We envisage that results from this study pave the way to rapidly but safely move between pre-clinical and clinical translational studies applying combined gene/cell therapy protocols to address the complexity of GLD and similar LSDs.

Results

In this study, we tested the efficacy of neonatal NSCT and LV-mediated IC GT (5,29) in clinically relevant combinatorial settings with BMT. The timing of administration was determined based on the rapid progression of the disease in Twi mice. Thus, lethal irradiation and BMT were performed at PND6 and PND7, respectively, the earliest time possible after neonatal NSCT or IC GT. Untreated (UT), NSCT, IC GT-treated Twi mice, Twi mice transplanted with total BM from wild-type (WT) tgGFP mice as well as UT, NSCT and BMT WT age-matched littermates were used as controls to compare the outcome of combined versus single treatments (Supplementary Material, Fig. S1).

Synergic effect of combined treatments in enhancing lifespan of Twi mice

The Kaplan–Meier survival curves for all treatment groups are reported in Figure 1A. The median survival of UT Twi mice was 41 days, with a wide interval (20–54 days) that reflects the variability

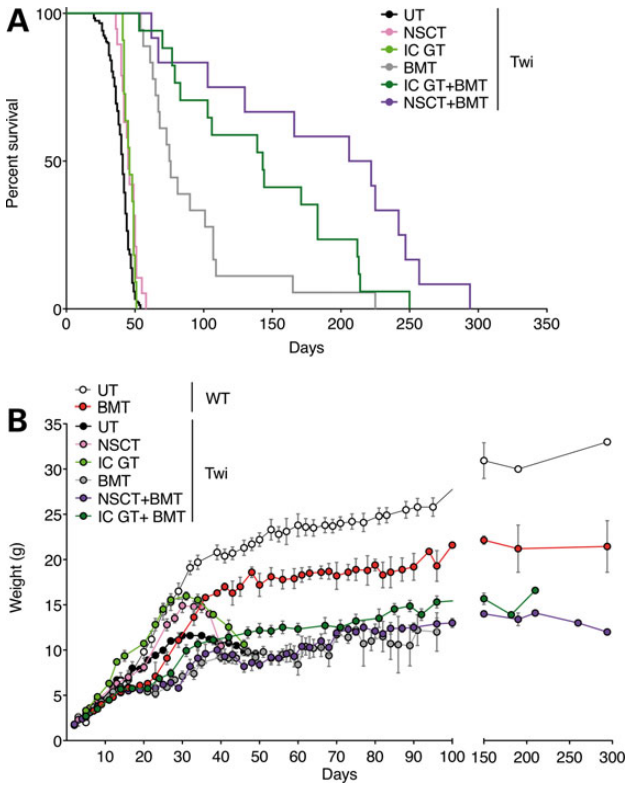

Figure 1. Synergic enhancement of lifespan and body weight stabilization upon combined treatments in Twi mice. (**A**) Kaplan–Meier survival curves of treated and UT Twi mice. UT Twi, $n = 240$; NSCT Twi, $n = 19$; BMT Twi, $n = 18$; NSCT + BMT Twi $n = 12$; IC GT Twi, $n = 11$; IC GT + BMT Twi, $n = 17$. Data analyzed by Log-Rank (Mantel–Cox) test; $P = 0.0273$ (IC GT), $P = 0.0005$ (NSCT) and $P < 0.0001$ (BMT, NSCT + BMT and IC GT + BMT) versus UT Twi; $P = 0.0007$ (NSCT + BMT) and $P = 0.0163$ (IC GT + BMT) versus BMT Twi; $P = 0.0513$ NSCT + BMT Twi versus IC GT + BMT Twi. (**B**) Body weight of treated Twi mice and UT controls was monitored starting at PND2. BMT WT mice were used as control to assess the effect of irradiation on body growth.

of the disease progression. NSCT and IC GT alone resulted in moderate but consistent improvement of median survival (45 and 46 days, respectively). A significant enhanced benefit was observed in BMT Twi mice (median lifespan of 75.5 days, with two treated animals living beyond PND110) but only combined treatments significantly extended the average survival of Twi mice, which displayed a median survival of 214 days (NSCT + BMT) and 143 days (IC GT + BMT) with the majority of treated mice living beyond PND110. The improved benefit of BMT and combined treatments was also evident in terms of body weight (Fig. 1B). In contrast to the stable decrease in body weight observed in Twi mice starting from PND21 (UT) or PND30 (NSCT and IC GT), body weight of BMT and combined-treated Twi mice slightly increased over time from PND30, with long-lived mice reaching up to 70% of the weight of BMT WT littermates (note that irradiation jeopardized weight gain in both WT and treated Twi mice). Importantly, combined-treated Twi mice displayed little twitching, absent or mild hind-limb stiffness, maintained the ability to walk and feed independently as well as typical explorative activity at time-points that were far beyond the median lifespan of affected littermates treated with BMT alone (Supplementary Material, Videos S1–S6).

Timely targeting of CNS, PNS and peripheral organs in combined-treated Twi mice

Mice were examined to evaluate: (i) cell engraftment, migration and differentiation of NSCs; (ii) efficacy of transduction upon IC GT; (iii) engraftment of HCs in the hematopoietic compartment; (iv) engraftment of HC myeloid progeny in CNS tissues.

In line with our previous study (29) transplanted NSCs were found lining the lateral ventricles as early as 5 days after injection (not shown). At PND40 and thereafter, GFP$^+$ NSCs were found preferentially in the forebrain subventricular region and subcortical WM tracts (Fig. 2A), with few if any cells in the cerebellum (CB) and spinal cord (SC). The yield of engraftment ranged between 0.3 and 3.5%, as reported in previous studies (29,30), being stable over time and comparable in all treatment groups (Fig. 2B). Within the GFP$^+$ NSC population, ~35% of total cells counted were astrocytes [glial fibrillary acidic protein (GFAP)], 8% were neurons (PSA-NCAM), 10% were oligodendrocytes (APC), while the remaining cells were negative for these lineage markers and maintained immature features, with no obvious differences related to treatment (NSCT or NSCT + BMT) or time after treatment (PND40 or PND80). Of importance, progressive maturation of engrafted NSCs was observed over time, as NSC progeny found in PND80 and long-lived NSCT + BMT Twi mice were appropriately integrated as mature neurons in the olfactory bulb (OB) and hippocampus (Fig. 2C), as astrocytes (Fig. 2D) and mature oligodendrocytes (Fig. 2E) in WM tracts. These results suggest that engraftment, longstanding survival and differentiation of transplanted NSCs are not affected by the irradiation protocol, by donor-derived HCs or by the pathological Twi environment. Importantly, we never detected foci of hyperproliferation, abnormal cell masses of donor origin or engrafted NSCs expressing the proliferation marker Ki67, at any time point considered ($n = 9$ mice; up to PND294).

Finally, we observed robust transduction of endogenous cells and widespread transgene diffusion, mainly along WM tracts, upon neonatal IC GT. We assessed LV transduction efficiency in LV.GFP-injected mice by counting the number of GFP$^+$ cells in serial coronal sections comprising the injection site (Fig. 2F), showing ~5–10% of GFP$^+$ cells on the total number of nuclei. These results are in line with our previous studies, in which we also demonstrated similar transduction efficiency of LV.GFP and LV.GALC (5).

Given the multi-organ pathology that characterizes Twi mice, a robust donor chimerism upon BMT is critical to ensure relevant therapeutic benefit. We assessed the donor chimerism by quantifying GFP$^+$ HCs in peripheral blood (PB) and BM of treated mice. Our results showed robust and stable HC engraftment (65–100%) in BMT WT mice as well as in BMT and combined-treated Twi mice analyzed at different ages (from PND20 to PND294; Fig. 3A).

We then evaluated the time-course engraftment of HC-derived myeloid cells in brain tissues. The different morphology and distribution of engrafted HCs as compared with NSCs together with the expression of cell lineage-specific markers allowed us to reliably differentiate between the two different GFP$^+$ cell populations. We observed time- and region-dependent HC engraftment in CNS tissues. In the telencephalon (TEL), few round-shaped CD45$^+$ cells were detected starting from PND20 in BMT and NSCT + BMT Twi mice, close to or inside blood vessels, almost exclusively in the cortex and choroid plexuses (Fig. 3B). At PND30 and PND40 HC-derived cells progressively increased in number and preferentially localized in cortical regions, showing small cell body and thin processes, in concomitance with downregulation of CD45 expression and upregulation of Iba1 expression, an indication of progressive maturation towards brain-resident myeloid cells (Fig. 3C). While NSCs were hardly found in the posterior CNS, HC engraftment in the SC and CB was robust as early as PND20. Iba1$^+$ myeloid progeny were preferentially distributed along WM tracts (Fig. 3D and E), many of them displaying enlarged cell body and thick processes, suggestive of an activated phenotype. At PND80 the presence of donor-derived myeloid cells was massive in all CNS regions of BMT and NSCT + BMT Twi mice. Importantly, this substantial engraftment was maintained over time, in conjunction with more pronounced differentiation of donor-derived cells, occasionally displaying an activated morphology in the WM tracts of TEL (Fig. 3F). At late time points up to 70% of GFP$^+$ myeloid cells expressed Ki67 and/or cleaved-caspase 3 (C3) (Supplementary Material, Fig. S2), suggesting that a balance between cell proliferation and apoptosis was maintaining homeostasis of donor-derived myeloid progeny in LT engrafted mice. The kinetics and the yield of HC engraftment and myeloid differentiation in CNS tissues were comparable in BMT and NSCT + BMT mice, suggesting that engrafted NSCs do not impact on these processes. In line with the capacity of HC myeloid progeny to colonize the PNS and visceral organs (31,32) we found numerous GFP$^+$ donor-derived cells in the sciatic nerve (SN; Fig. 3G) and liver (Fig. 3H) of BMT and NSCT + BMT Twi mice analyzed at PND80 and LT, without evident differences related to treatment.

Despite BMT Twi and BMT WT mice showed comparable hematopoietic chimerism and repopulation of the liver macrophage compartment (see Fig. 3A and Supplementary Material, Fig. S3), few donor-derived HCs were found in the CNS of BMT WT mice analyzed at PND80, almost exclusively localized in the choroid plexuses (Supplementary Material, Fig. S3). These results strongly suggest that pathology-driven mechanisms underlie the peculiar HC engraftment, myeloid differentiation and turnover observed in the CNS of transplanted Twi mice.

In summary, our combined protocols exploiting the robust LV-platform to directly transduce CNS cells and the complementary biological features of NSCs and HCs allow specific, extensive, timely and long-lasting targeting of multiple organs/tissues that undergo progressive storage and/or degeneration in Twi mice.

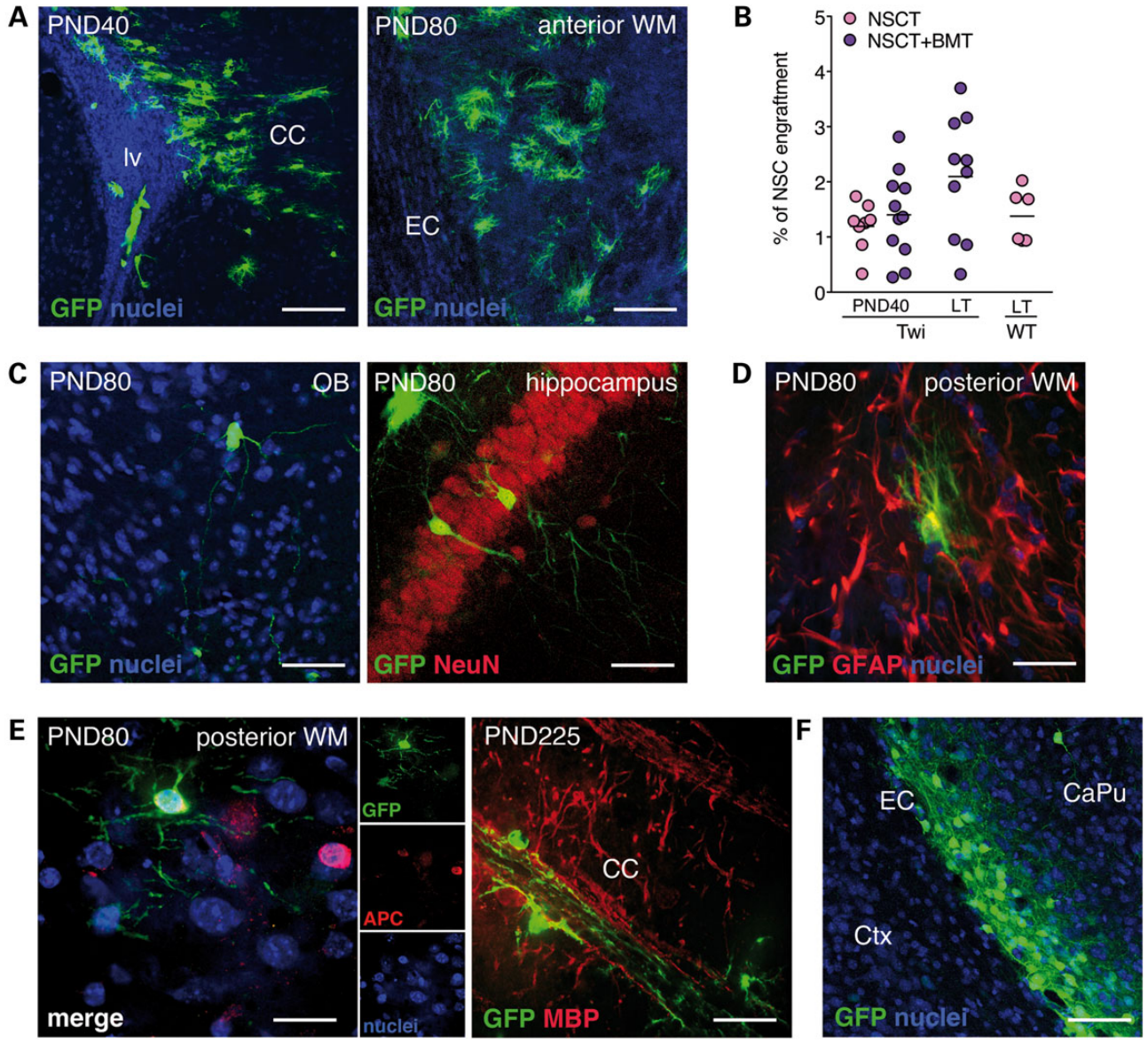

Figure 2. Stable engraftment of transplanted NSCs and robust tissue transduction upon IC GT. (**A**) Representative confocal images showing engrafted NSCs in the forebrain subventricular region and subcortical WM tracts. CC: corpus callosum, EC: external capsule; lv, lateral ventricle. (**B**) Comparable yield of NSC engraftment in NSCT WT mice and in NSCT and NSCT + BMT Twi mice, from PND40 and at LT (up to PND294). (**C–E**) Representative confocal images showing engrafted NSC-derived neurons in the olfactory bulb (OB) and hippocampus (C; NeuN), astrocytes (D; GFAP) and oligodendrocytes (E; APC, MBP) in WM tracts of NSCT + BMT Twi mice analyzed at PND80 and at PND225. (**F**) Representative confocal picture showing transduced cells in PND40 Twi mice upon neonatal LV.GFP injection. CaPu: Caudate Putamen, Ctx: cortex. Scale bars: (A) 100 μm; (C, D and F) 60 μm; (E) left panel: 40 μm, right panel: 60 μm.

Rapid and stable reconstitution of GALC activity in the CNS and periphery of treated Twi mice

We evaluated in a time-course analysis the specific GALC activity in the CNS, PNS and periphery of treated Twi mice and UT controls. We showed that NSCT and IC GT supply 30–40% of physiological GALC activity in CNS tissues starting from 3 days after treatment. This ensured significantly higher levels of GALC activity in NSCT and IC GT as compared with BMT Twi mice as early as PND10 (Fig. 4A). Starting from PND20 GALC activity was stable and comparable in all treatment groups, with no apparent additive or synergic effect in combined-treated Twi mice (Fig. 4A). These apparent counterintuitive results suggest tight regulation of GALC expression/activity in CNS tissues, a hypothesis that is supported by several observations: (i) the modest (if any) increase of GALC activity in CNS tissues of WT mice upon transplantation of GALC-overexpressing NSCs or IC GT; (ii) the comparable levels of GALC activity in Twi CNS tissues following one or three intraparenchymal injections of LV.GALC; (iii) the physiological GALC activity in CNS tissues of transgenic Twi bearing 4–6 copies of the wt *galc* gene (Supplementary Material, Fig. S4).

Of note, HC provided up to physiological levels of GALC activity in the PNS (SN), liver and BM of combined-treated Twi mice (Fig. 4B).

Long-term clearance of storage in CNS, PNS and visceral organs of combined-treated Twi mice

In order to assess the effect of the different approaches in preventing/halting disease progression, we performed comprehensive time-course analyses examining relevant pathological

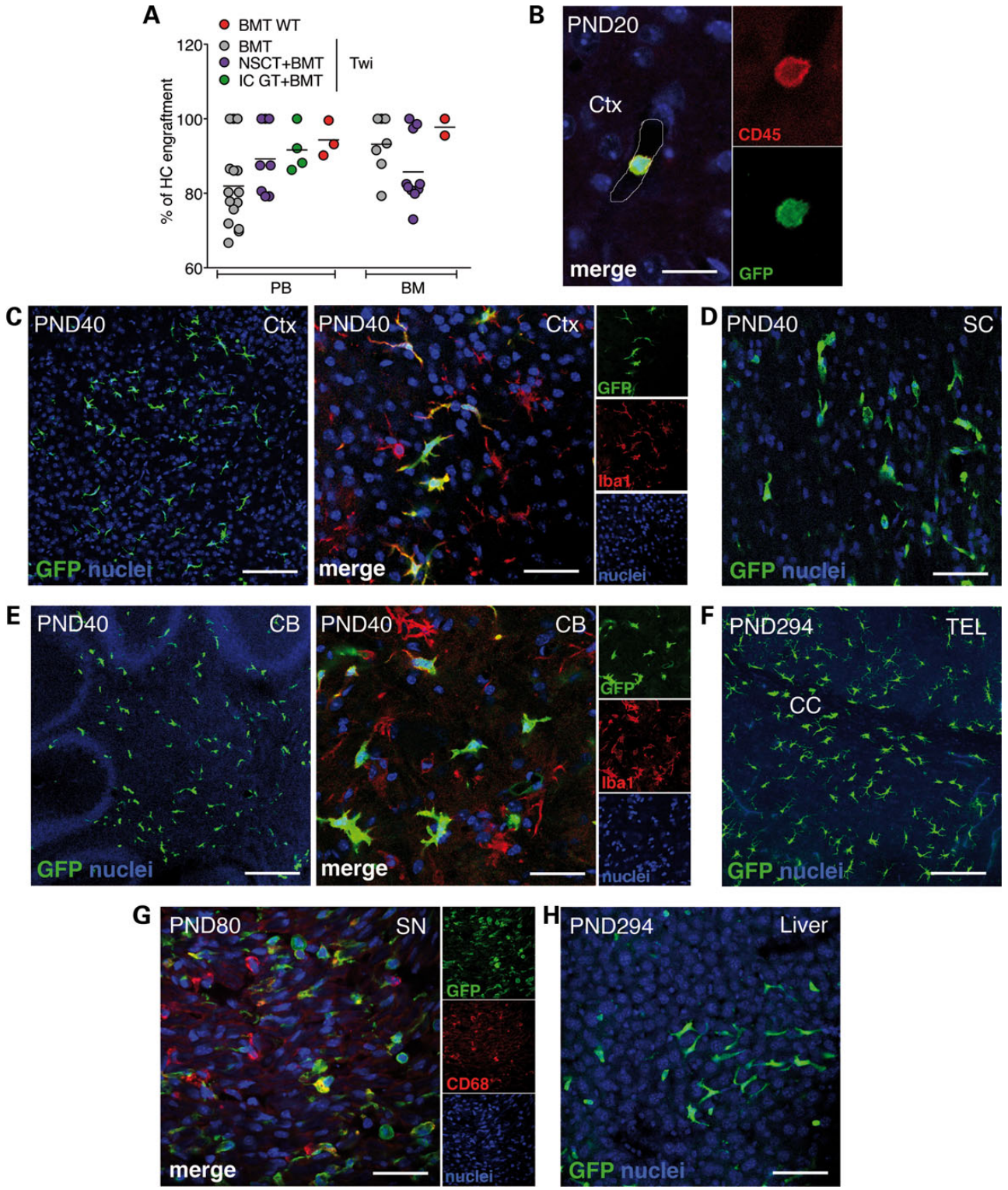

Figure 3. Robust time-dependent, caudal to rostral HC engraftment upon BMT. (**A**) Stable HC engraftment in BM and PB of recipient mice. (**B**) GFP$^+$CD45$^+$ cells in telencephalic vessels of BMT Twi analyzed at PND20. (**C**) GFP$^+$ HC myeloid progeny expressing Iba1 in cortical regions of BMT Twi analyzed at PND40. (**D** and **E**) Massive engraftment of GFP$^+$Iba1$^+$ myeloid cells in the SC and CB (WM tracts) of BMT Twi mice analyzed at PND40. (**F**) GFP$^+$ HC myeloid progeny repopulates the TEL of LT NSCT + BMT Twi. (**G**) GFP$^+$ macrophages (CD68) in the SN of BMT Twi mice analyzed at PND80. (**H**) GFP$^+$ donor-derived cells engrafted in the liver of LT NSCT + BMT Twi mice. Scale bars: (B) 30 μm; (C) left panel: 250 μm, right panel: 60 μm; (D) 60 μm; (E) left panel: 250 μm, right panel: 60 μm; (F) 250 μm; (G and H) 60 μm.

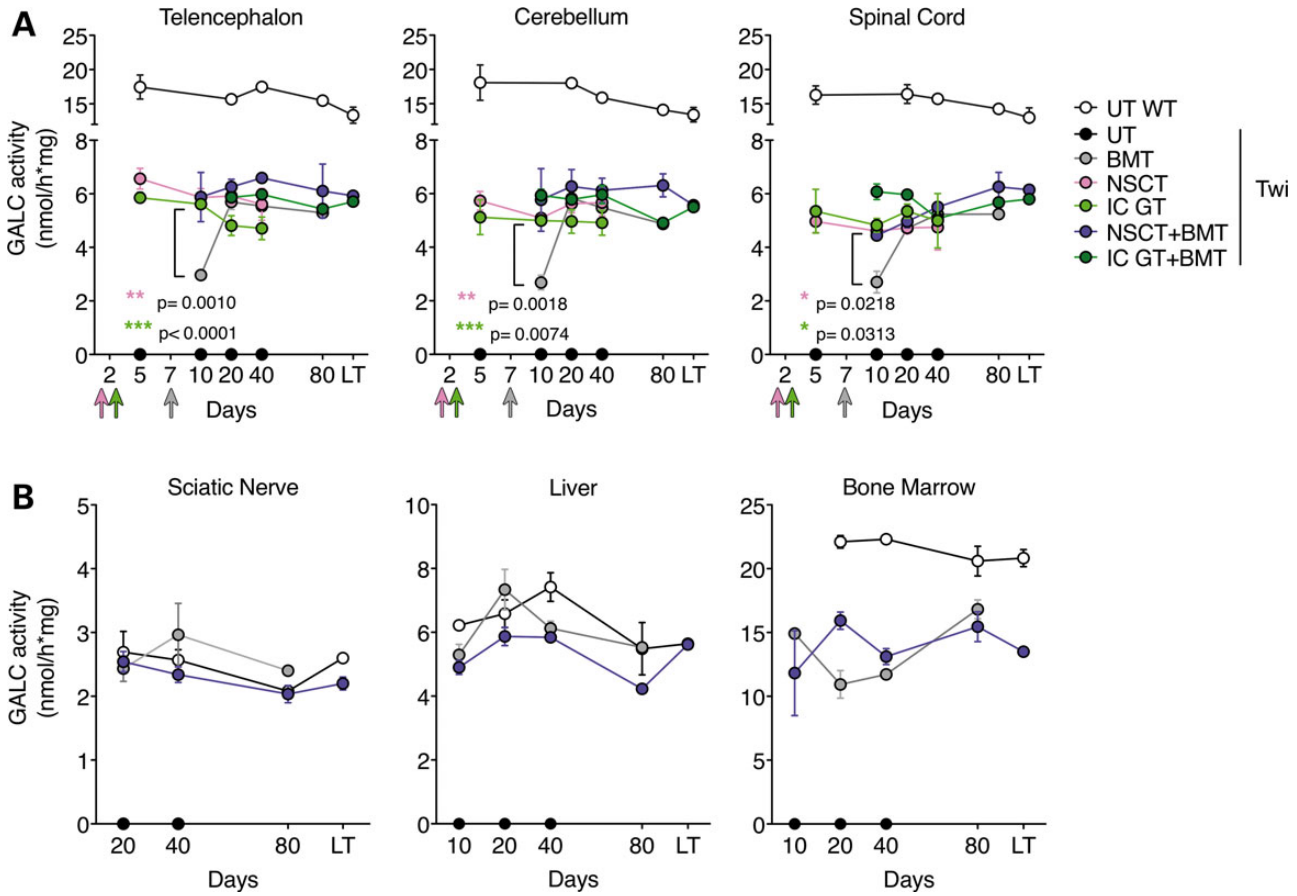

Figure 4. Rapid and stable reconstitution of GALC activity in the CNS and peripheral organs of treated Twi mice. Time-course analysis of GALC enzymatic activity in CNS tissues (**A**), PNS, liver and BM (**B**) of single- or combined-treated Twi mice and UT controls. Arrows indicate the time of treatment, according to the colour code reported in the figure legend. Data are expressed as mean ± SEM; $n = 3$–6 mice/group (PND5 to PND40); $n = 3$ mice/group (PND80 and LT). GALC activity of NSCT or IC GT Twi and BMT Twi at PND10 (A) are compared using the unpaired Student's *t*-test. Asterisks indicate statistical significance according to the colour code reported in the figure legend.

hallmarks. Based on our previous studies showing a comparable contribution of neonatal NSCT and IC GT in providing metabolic correction and ameliorating CNS pathology in Twi mice (5,29) and on data presented here thus far showing similar outcome of the two combined treatments, we focused the following analyses on NSCT + BMT Twi mice, showing only selected readouts and relevant time points for IC GT + BMT Twi mice.

We first assessed the intracellular galactolipid storage using lectin histochemistry (33). Lectin$^+$ storage was strongly increased in CNS tissues of UT Twi mice as compared with age-matched WT littermates, in a region-dependent manner (SC > CB > TEL) (Fig. 5A). The rapid GALC supply provided by engrafted NSCs in the TEL and the combination of local and transported GALC enzyme provided by BMT and NSCT, respectively, in CB and SC, likely explain the significant 50–70% reduction of storage detected in all CNS regions of NSCT + BMT Twi mice analyzed at PND40. Importantly, galactolipid storage in LT NSCT + BMT Twi mice was hardly distinguishable from the physiological levels found in age-matched WT littermates (Fig. 5A and B).

As a consequence of GALC deficiency, Psy accumulates up to 100-fold the physiological levels in nervous tissues of Twi mice, with age-dependent progression and caudal-to-rostral accumulation (Supplementary Material, Fig. S5). Our results showed that Psy levels in NSCT Twi mice at PND40 are indistinguishable from those of UT Twi littermates, while a significant 50–70% reduction was observed in BMT and NSCT + BMT Twi mice (Fig. 5C), indicating donor-derived HCs as key players in Psy clearance. Importantly, active clearance of Psy was maintained or even enhanced over time, as indicated by the substantial reduction of Psy levels with respect to UT Twi levels found in all CNS regions (up to 90% reduction), in PNS (30–50% reduction) and in the liver (up to 90% reduction) of long-lived combined-treated Twi mice (from PND150 to PND294), including those BMT Twi mice that we had the opportunity to analyze at the moribund state (from PND85 to PND144). Importantly, NSCT + BMT and IC GT + BMT provided similar stable metabolic correction in CNS and periphery (Fig. 5C).

Delayed progression of astrogliosis in CNS tissues of NSCT + BMT Twi mice

We then performed GFAP staining to monitor the activated state of astroglial cells, quantifying GFAP-immunopositive signal in treated Twi mice as well as UT Twi and WT controls at different time points. Our results showed that astrogliosis is reduced in all treatments groups assessed at PND40, with some variability associated to the type of treatment and the CNS region considered. In particular, a significant reduction of GFAP$^+$ signal was detected in the TEL and CB of NSCT and NSCT + BMT Twi mice, likely as a consequence of the early enzymatic supply and, possibly, of the anti-inflammatory/immunomodulant activity provided by locally engrafted NSCs. In treated mice

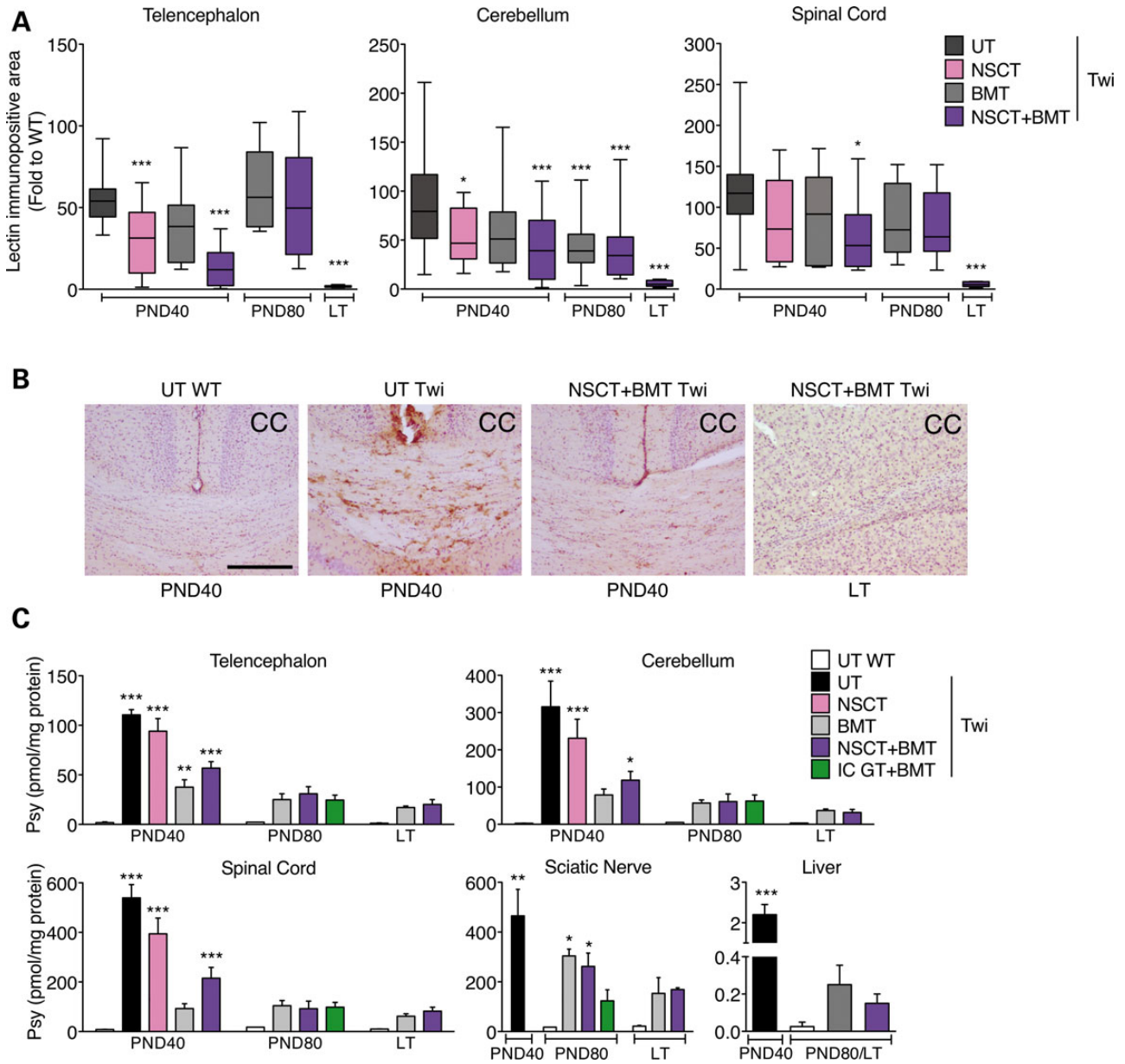

Figure 5. Long-term clearance of tissue storage in combined-treated Twi mice. (**A**) Lectin positive area in CNS tissues of treated Twi mice and UT controls. Data are in pixels and expressed as fold to WT. Results from BMT WT and UT WT mice have been pooled due to superimposable results obtained from the two groups; $n = 3–5$ mice/group, 5 slices/animal, 3–5 fields/slice. Data are expressed as mean + SEM and analyzed by One-way ANOVA followed by Dunnet's post-test comparing all groups against UT Twi (*$P < 0.05$, ***$P < 0.001$). (**B**) Representative pictures of lectin staining in the CC of UT controls and NSCT + BMT Twi at PND40 and LT; scale bar: 350 μm. (**C**) Time-course analysis showing progressive clearance of Psy storage in treated as compared with UT Twi mice. $n = 3–7$ mice/group. Data are expressed as mean + SEM and analyzed by One-way ANOVA followed by Dunnet's post-test comparing all groups against UT WT (*$P < 0.05$, **$P < 0.01$, ***$P < 0.001$).

analyzed at PND80 and LT we consistently observed that GFAP expression levels were similar or higher as compared with those measured in UT Twi at PND40. These results strongly suggest a transient benefit of treatments in counteracting astrogliosis, pointing to persistent neuroinflammation in long-lived treated Twi mice (Fig. 6A and B).

Efficient prevention of apoptosis and improved myelination in the CNS of combined-treated mice

Psy storage leads to upregulation of C3 and apoptosis of oligodendrocytes and neurons (34,35). We found considerable numbers of apoptotic cells displaying oligodendroglial morphology in the SC of PND40 UT Twi (Fig. 7A), the CNS region showing the highest levels of Psy at any age considered (see Fig. 5C). NSCT alone was not effective in reducing the number of apoptotic cells. Combined treatment was more advantageous than BMT alone in decreasing apoptosis at PND40, while complete rescue to physiological levels was observed at PND80 in both treatment groups (Fig. 7B).

Twi mice display a mild CNS demyelination, with modest oligodendrocyte loss and derangement of the remaining cells along the WM tracts. Our previous studies showed that western blot analysis assessing myelin basic protein expression, Kluver–

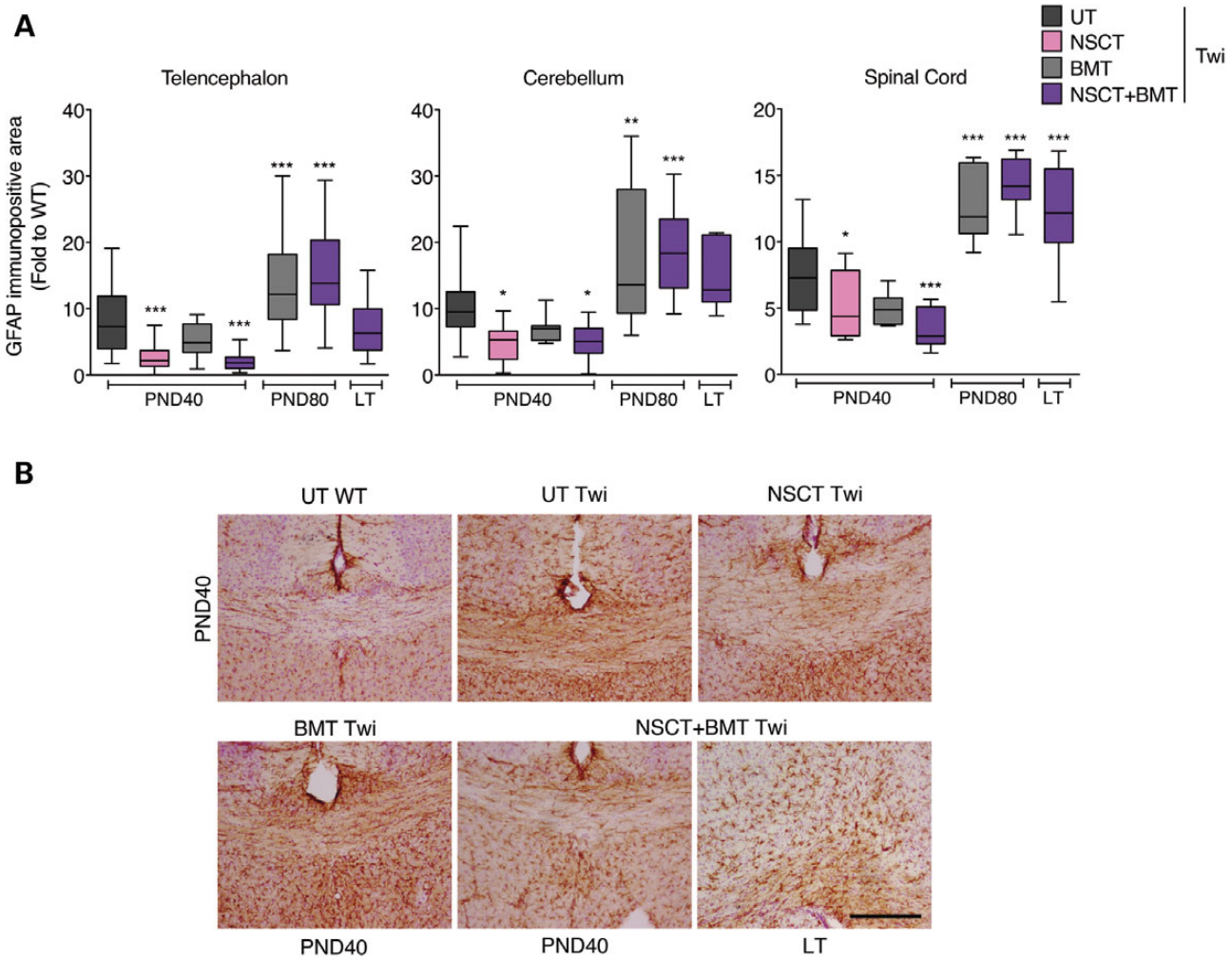

Figure 6. Delayed astrogliosis in CNS tissues of combined-treated Twi mice. (**A**) GFAP-immunopositive area in CNS tissues of treated Twi mice and UT controls. Data are in pixels and expressed as fold to WT. Results from BMT WT and UT WT mice have been pooled due to superimposable results obtained from the two groups; $n = 3$–5 mice/group, 5 slices/animal, 3–5 fields/slice. Data are expressed as mean + SEM and analyzed by One-way ANOVA followed by Dunnet's post-test comparing all groups against UT Twi (*$P < 0.05$, **$P < 0.01$, ***$P < 0.001$). (**B**) Representative pictures of GFAP staining in the CC of UT controls and treated Twi mice analyzed at PND40 and LT. Scale bar: 350 μm.

Barrera staining and immunohistochemistry (IHC) for the oligodendrocyte-specific marker GST-π could hardly quantify those minor differences (29,35). Thus, we reasoned that assessing the time-course expression of oligodendrocyte-specific genes by qPCR could highlight more subtle alterations between WT and Twi and, consequently, between treated Twi mice and UT littermates. We chose to analyze three genes that were previously validated as differentially expressed in the original Twitcher mouse as compared with WT littermates, namely cgt (uridine diphosphate-galactose:ceramide transferase), the key enzyme in galactolipid biosynthesis, and the structural proteins mag (myelin associated glycoprotein) and plp1 (proteolipid protein 1) (36). In line with this work, our results showed that expression of *cgt*, *mag* and *plp1* were downregulated from 40 to 65% and from 55 to 90% in the TEL and SC, respectively, of end-stage UT Twi mice (PND40) as compared with age-matched WT littermates (Fig. 7C). While only modest rescue of gene expression was observed in all treatment groups analyzed at PND40, mRNA levels were rescued to physiological levels in BMT and NSCT + BMT Twi analyzed at PND80. This benefit was lost at longer time points (Fig. 7C), suggesting damage to myelinating cells in long-lived treated Twi mice.

Prevention of neuronal damage in CNS tissues of combined-treated Twi mice

Activating transcription factor 3 (*ATF3*) is an adaptive response gene whose activity and expression are regulated by stressful stimuli and in response to neuronal injury (37). We previously reported region- (SC > CB) and age-dependent (PND40 > PND30) upregulation of *ATF3* mRNA in Twi mice when compared with WT littermates (35). We showed here that *ATF3* mRNA levels are significantly upregulated also in the TEL of PND40 UT Twi mice (Fig. 7D). Interestingly, Twi mice receiving combined-treatment showed a more efficient downregulation of *ATF3* mRNA levels than those receiving single treatments alone in the CB and SC, the latter region showing the highest *ATF3* upregulation. In the TEL, the putative neuroprotective activity of locally engrafted NSCs might explain the comparable benefit observed in NSCT and NSCT + BMT Twi mice (Fig. 7D).

We found a significant increase in the number of neurons overexpressing ATF3 protein in the SC of Twi mice as compared with WT littermates at PND40 (Fig. 7E), and identified motor neurons in the ventral horns as the most susceptible neuronal population (Fig. 7F). Both BMT and NSCT + BMT were effective in completely preventing ATF3 expression in SC tissues of mice

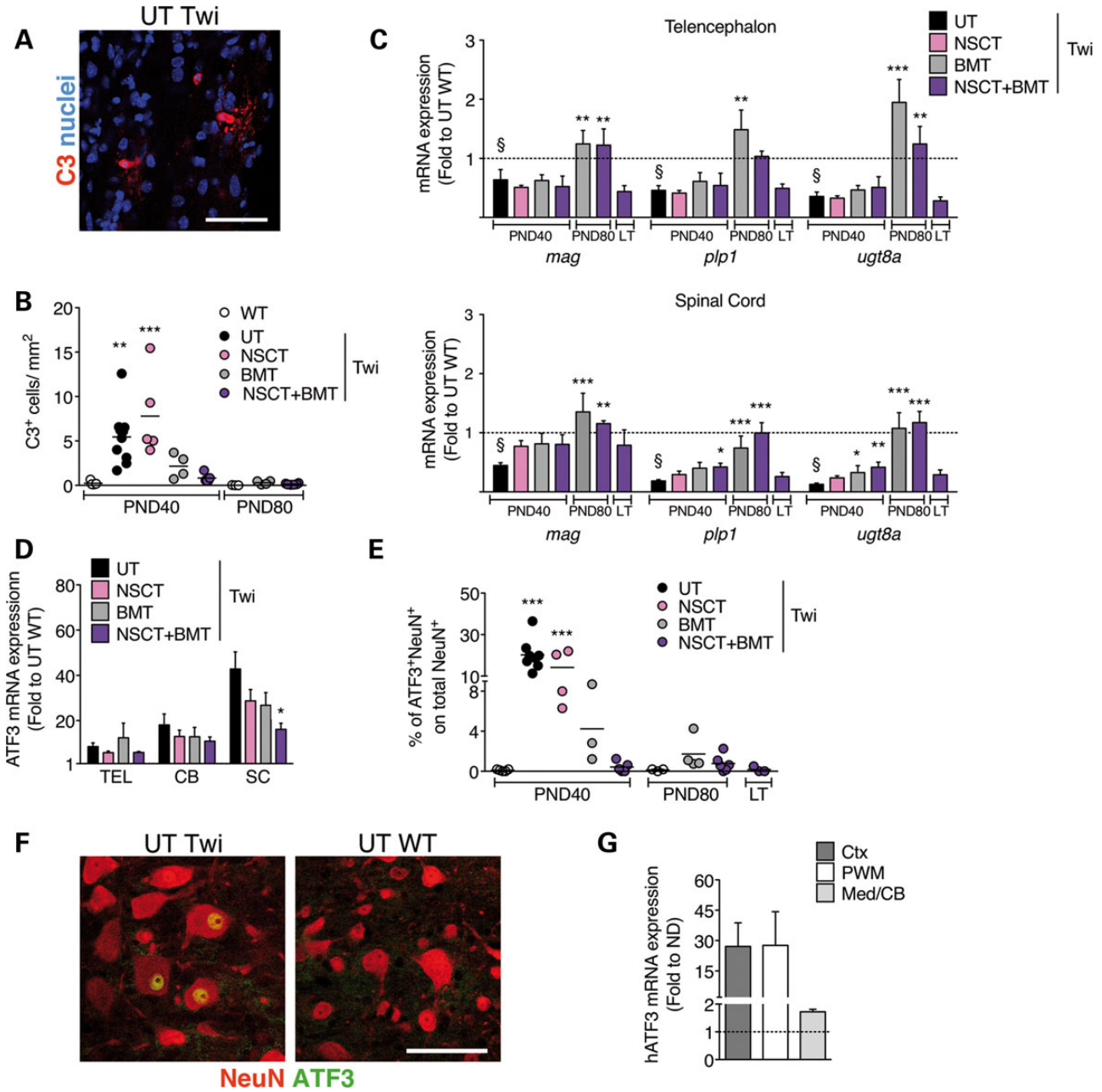

Figure 7. Rescue of apoptosis, myelination and neuronal stress in the CNS of treated Twi mice. (**A**) Representative confocal picture showing an oligodendrocyte-like apoptotic ($C3^+$) cells in the SC of UT Twi mouse at PND40. Scale bar: 60 μm. (**B**) Significant reduction of $C3^+$ cells in the SC of NSCT + BMT Twi mice. Data are analyzed by One-way ANOVA followed by Dunnet's post-test comparing all groups against UT WT (**$P < 0.01$, ***$P < 0.001$). (**C**) Time-course analysis of mRNA expression of *Mag*, *Plp1* and *Ugt8a* in the TEL and SC of treated animals. Data are normalized on *Gapdh*, expressed as fold ($2^{-\Delta\Delta CT}$) to age-matched UT WT (set as 1); $n = 3$–8 mice/group. Data (ΔΔCT values) are analyzed by One-way ANOVA followed by Dunnet's post-test comparing all groups against UT Twi (*$P < 0.05$, **$P < 0.01$ and ***$P < 0.001$ versus UT Twi, §$P < 0.05$ versus UT WT). (**D**) Significant reduction of *ATF3* mRNA levels in the SC of NSCT + BMT Twi analyzed at PND40. Data (mean + SEM) are normalized on *β-actin* and expressed as fold ($2^{-\Delta\Delta CT}$) to age-matched UT WT (set as 1); $n = 4$–8 mice/group. Data (ΔΔCT values) are analyzed by One-way ANOVA followed by Dunnet's post-test comparing all groups against UT Twi (*$P < 0.05$). (**E**) Percentage of $ATF3^+$ SC neurons in treated Twi mice and controls. Data are analyzed by One-way ANOVA followed by Dunnet's post-test comparing all groups against UT WT (***$P < 0.001$). (**F**) Representative confocal picture of $ATF3^+$ neurons in the ventral horn of the SC in UT Twi mice. Physiological ATF3 expression is undetectable by IF assay in UT WT mice. Scale bar: 60 μm. (**G**) Upregulation of *hATF3* mRNA expression in CNS tissues from GLD patients ($n = 2$). Data (mean + SEM) are expressed as fold to normal donors (ND, set as 1; $n = 2$) after normalization on *hHPRT1*. Ctx: cortex, PWM: periventricular white matter, Med/CB: medulla/cerebellum.

analyzed at PND80 and LT, whereas the combined treatment resulted in stronger benefit as compared with BMT alone at PND40 (Fig. 7E), suggesting that synergy could be particularly important at the early time points.

Of note, by analyzing post-mortem CNS tissues from two GLD patients and two normal donors, we showed a variable but substantial upregulation of *hATF3* mRNA expression associated to the disease (Fig. 7G). These results strongly suggest that CNS

neuronal stress and consequent neuronal dysfunction might indeed contribute to human GLD pathology.

Enhanced preservation of myelinated axons in SNs of combined-treated Twi mice

In order to assess whether treatments were able to preserve myelin in peripheral nerves we performed morphometric analysis on SN of treated Twi mice and UT controls to assess the number, diameter and density of myelinated axons. Qualitative observations of nerve sections depicted a progressive loss of myelinated fibres together with extensive myelin and axon degeneration, and disorganized clusters of Remak bundles in UT Twi mice starting as early as PND10-PND20 as compared with age-matched WT littermates (Supplementary Material, Fig. S6). In Twi mice analyzed at PND30 and PND40 only small calibre axons (<2 μm) were preserved, which were often hypomyelinated (Supplementary Material, Fig. S6), while <10% of medium-large diameter fibres were spared. Despite nerves from BMT and BMT + NSCT Twi mice analyzed at PND80 still displayed dysmyelination, hypomyelination and reduced density of fibres (Fig. 8A), the number of myelinated axons was increased and we observed onion bulb formations suggestive of re-myelinating attempts. This amelioration was clearly enhanced in combined-treated as compared with BMT Twi mice, which more closely resembled symptomatic UT Twi mice (PND40). Interestingly, among NSCT + BMT Twi mice, three out of six animals showed higher number and increased density of myelinated fibres, indicating a better outcome of the treatment and an appreciable improvement towards the WT phenotype (compare NSCT + BMT Twi a and b with UT WT). Notably, qualitative observations on nerves from two long-lived NSCT + BMT Twi mice (PND225 and PND294) showed a phenotype comparable with that described in treated mice at PND80, suggesting that combined treatment prevented further myelin deterioration (Fig. 8A).

If we directly compare morphometric analyses of UT Twi mice at PND40 and treated Twi mice at PND80 (values of UT WT mice at PND40 and PND80 were superimposable) we observed better preservation of medium (3–5 μm; +150%) and large (>5 μm; up to +400%) fibres (Fig. 8B) as well as an overall increase in the density of fibres in combined-treated (+60%) as compared with UT Twi mice (Fig. 8C).

In order to determine the outcome of treatments on PNS and CNS functionality we performed neurophysiological evaluation of treated mice and UT controls at PND30, PND80 and LT. Demyelination and concomitant loss of axon insulation lead to the reduced motor nerve conduction velocity (MCV), increased central conduction time (CCT) and decreased amplitude of compound motor action potential (cMAP) in Twitcher mice (38,39). We showed an age-dependent increase of MCV in WT mice, consistent with the developmental maturation of PNS and CNS. No further changes occurred at later time points (Fig. 8D). UT Twi mice analyzed at PND30 showed severe slowing of MCV (≈7 m/s) as compared with age-matched WT controls (≈28 m/s). Despite the MCV measured in treated Twi mice (≈8 m/sec, regardless of the treatment or the age, PND294 being the last time point analyzed) was consistently slowed down as compared with that of age-matched WT (≈43 m/sec), it was stable and with no sign of further deterioration over time (Fig. 8D). This result is noteworthy since MCV is not even measurable in late stage UT Twi (PND40). The benefit provided by treatments was more evident by looking at the cMAP amplitude, which was not only stabilized but consistently increased in BMT and combined-treated Twi mice, in line with morphological data showing enhanced preservation of myelinated axons. The cMAP of treated Twi mice analyzed at PND80 was ≈40% of WT levels (to be compared with ≈15% of age-matched WT shown by UT Twi at PND30), and was maintained in mice analyzed at later time points (up to PND294) (Fig. 8E). The CCT increased from ≈3 ms in the WT (stable from PND30 up to PND294) to the aberrant value of ≈6 ms in UT Twi mice at PND30 (Supplementary Material, Fig. S7). A slight but appreciable decrease of CCT was observed in NSCT Twi mice at PND30 and no further deterioration was detected at PND80 and, more importantly, in LT NSCT + BMT Twi (up to PND294; Supplementary Material, Fig. S7).

Discussion

In this work, we provide proof-of-concept of efficacy, tolerability and clinical relevance of combining CNS-directed approaches (transplant of gene-corrected NSCs or LV-based IC GT) with BMT to correct the GLD phenotype in a mouse model that recapitulates the severity and rapid progression of the early infantile human disease.

The reliable assessment of additivity/synergy between two or more strategies depends on the consistent therapeutic outcome of single treatments. To this end, we took advantage of optimized protocols for NSCT (29), IC GT (5) and BMT/HSCT (32,40) in LSD murine models.

The efficacy of the combined approaches proposed here was firstly demonstrated by their synergy in enhancing the lifespan of Twi mice. Combined-treated mice significantly outperformed animals treated with either approach alone, living up to 9–10 months and maintaining stable body weight. Importantly, our video recordings clearly documented that although eventually mild tremor became apparent, combined-treated mice remained capable of moving with ease until the very last days of life. In stark contrast, animals treated with IC GT, NSCT and even BMT showed variable delay in the onset of symptoms but a sharp progression of disease, hardly distinguishable from that of UT Twi mice. To the best of our knowledge, our study reports the highest improvement of average lifespan upon combined therapies in GLD mice ever. In a prior study (25), Twitcher mice treated with six intracerebral injections of AAV2/5.GALC coupled with BMT showed enhanced survival (median lifespan: 123 days) but a sharp disease progression, comparable with that observed in our BMT Twi mice. Another study (28) reported enhanced survival (average lifespan: 120 days) in Twitcher mice treated with multiple AAV.rh10.GALC injections (one intrathecal, two systemic and six intracerebral), a protocol that is feasible in mice but has limited potential for clinical translation, due to safety concerns. In contrast, we tested here two minimally invasive CNS-directed approaches that have shown efficacy and favourable safety profile in GLD mice (5,29).

Both NSCT using prospectively isolated fetal hNSCs (41) as well as AAV-mediated IC GT (42,43) have entered clinical testing for neurodegenerative LSDs, with variable outcome in terms of safety and efficacy. We envisage that our data in mice (5,29) and recent results of the first-in-men LV-mediated IC GT trial (44), highlight a rationale for applying the LV-mediated GT platform to treat CNS pathology LSDs, possibly circumventing immune issues related to the use of AAVs (45) as well as ethical/technical issues related to heterologous hNSCT. Still, a potential advantage of NSCT over IC GT in a combinatorial setting might be the ability of transplanted gene-corrected NSCs, which are resistant to the toxic Twi environment (12), to exhibit a broad repertoire of potentially therapeutic actions (46), including the modulation of the host environment and immune system

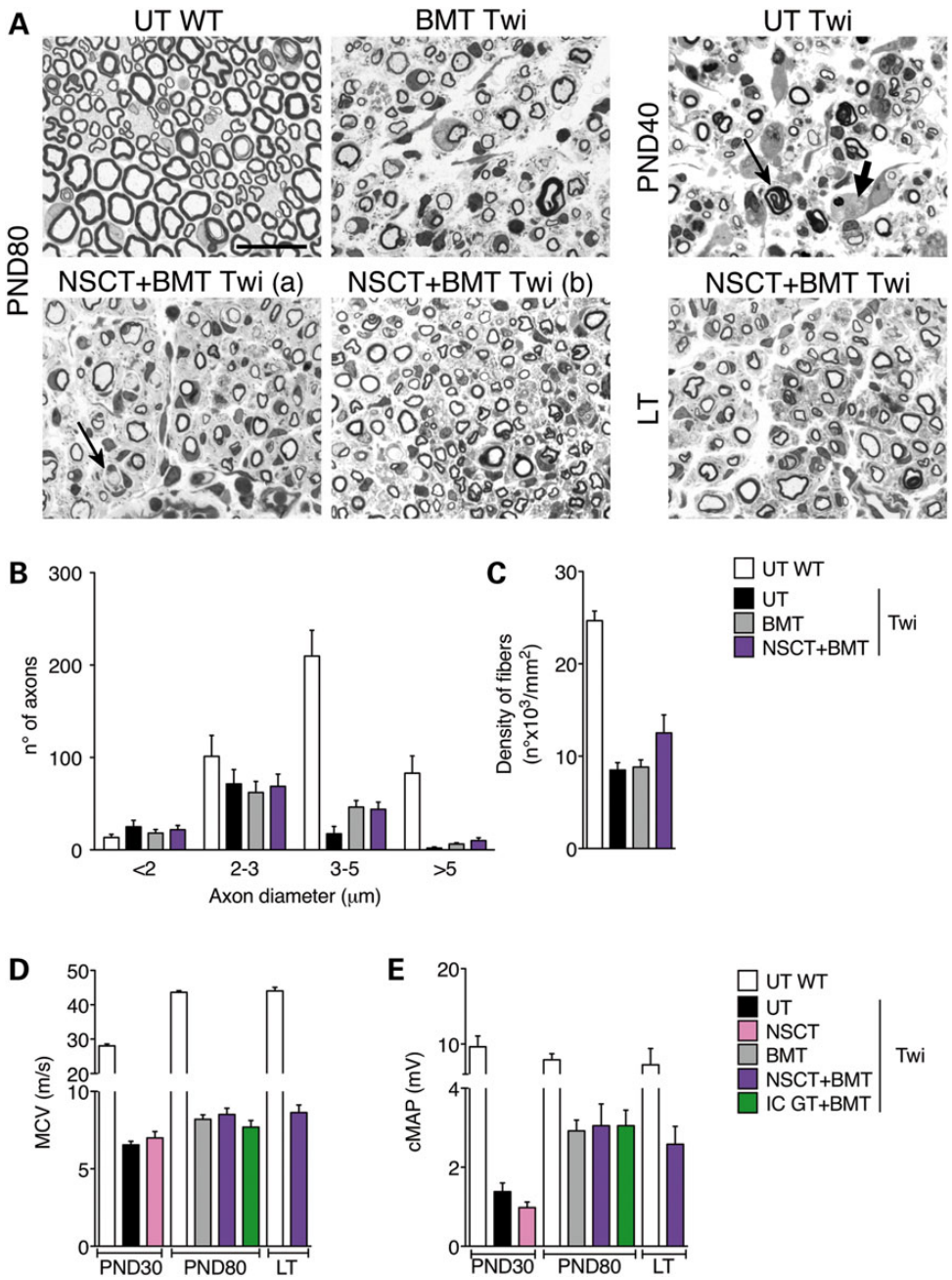

Figure 8. Enhanced preservation of myelinated axons in SNs of combined-treated Twi mice. (**A**) Representative pictures of SN sections of treated Twi mice at PND80 to be compared with age-matched WT mice and UT Twi mice at PND40, which is characterized by extensive loss of axons, dysmyelination (thin arrow), and active macrophages (thick arrow). NSCT + BMT Twi mice present with (a) similar density or (b) increased number and density of myelinated fibres as compared with BMT Twi mice, indicating re-myelination attempt, as also suggested by onion bulb formation [arrow in (a)]. Density of myelinated fibres is preserved in LT NSCT + BMT Twi mice. Scale bar: 10 μm. (**B**) Distribution of axon diameters showing preservation of medium-large calibre axons (3–5 μm and >5 μm) in BMT and NSCT + BMT Twi mice at PND80. (**C**) Density of fibres is increased in NSCT + BMT Twi mice at PND80. In (B and C) values related to UT Twi mice at PND40 are included as control; $n = 5–6$ mice/group. (**D** and **E**) Neurophysiological evaluation of treated Twi mice and UT controls at PND30, PND80 and LT showing long-term stabilization of MCV (D) and amelioration of cMAP amplitude (E) upon BMT and combined treatments. Data are expressed as mean + SEM; $n = 3–13$ mice/group, bilateral measures.

(29,47–49). Our data show similar long-term benefit of NSCT and IC GT in combination with BMT, despite a lower median survival observed in IC GT + BMT Twi mice. We may hypothesize that NSCs could confer a local advantage, protecting neuronal and glial precursor cells from the precocious functional impairment that has been reported in early post-natal GLD mice (34,50), as well as in affected infants (51,52).

The optimal efficacy of BMT was crucial to provide enhanced benefit in combinatorial settings. Full myeloablative conditioning accounted for the robust and stable hematopoietic chimerism achieved in BMT mice in this study (65–100%) as compared with the moderate engraftment (3–35%) reported in previous studies (23,25,26,53). This resulted in considerable repopulation of CNS and PNS tissues by HC myeloid progeny, allowing the

reliable assessment of BMT contribution to the therapeutic outcome. While NSC engraftment and survival were neither favoured nor hampered by the disease environment, HCs massively infiltrated the posterior CNS regions, that are most affected by the pathology and devoid of NSCs, highlighting a causative effect of GLD disease environment in priming HC recruitment to the CNS. Indeed, it is known that HC myeloid progeny poorly reconstitute CNS tissues in WT mice because the resident pool of microglial cells is largely self-sustaining (54,55). Importantly, the time-, region-, cell-type specific, complementary pattern of NSC and HC engraftment allowed the timely delivery of a functional GALC enzyme in the time-window in which Twi mice, despite being asymptomatic, progressively accumulate toxic substrates (34,50,56).

A closer look to the kinetics of GALC activity reconstitution highlighted two counterintuitive results: (i) CNS GALC activity upon BMT is stable between PND20 and PND80, despite the progressive increase of HC engraftment; (ii) combined treatments do not result in additive/synergic GALC activity. Our data provide indirect evidence that GALC activity in CNS tissues may be tightly regulated by yet undefined mechanisms. A deeper understanding of GALC structure, biochemistry and regulatory pathways would help understanding the mechanism underlying these puzzling observations.

The great benefit achieved in our study indicated proficiency of combined treatments in counteracting tissue damage at relevant disease sites. On the other hand, combined therapies did not definitely prevent disease progression, implying that some aspects of the complex GLD pathology might be more refractory to correction than others, with important implications for potential clinical translation. We provide here the first attempt ever to address these aspects systematically and comprehensively.

We examined glycolipid and Psy accumulation as primary pathological correlates of disease progression. Besides documenting an advantage of combined treatments short-term after transplant, we observed a dramatic reduction of toxic storage in the CNS and, to a minor extent, in the PNS of long-lived BMT and combined-treated mice. Still, low levels of Psy in CNS tissues (comparable with those measured in asymptomatic UT Twi mice at PND10) (50) might sustain a chronic inflammatory response and hamper remyelination attempts. This would explain the persistent/progressive activation of astrocytes and myeloid cells and the downregulation (after a transient rescue to physiological levels) of myelin-specific genes in long-lived combined-treated mice. We envisage that while the rapid GALC supply and the by-stander effects (immunomodulation, neuroprotection) exerted by engrafted HC progeny (57,58) may promote oligodendrocyte survival, high intracellular levels of functional GALC might be necessary to build and maintain functional myelin. A similar requirement might interest also Schwann cells. Indeed, regardless the complete enzymatic rescue, residual Psy levels in SNs of long-lived combined-treated mice strongly suggest suboptimal metabolic correction of this compartment. Storage and progressive functional impairment of PNS are present in asymptomatic GLD infants (56,59), with only mild and transient amelioration provided by HSCT (21,60,61). In Twi mice mild PNS impairment was already present at PND10 and relentlessly progressed. The similar effect of BMT and combined-treatments in stabilizing or enhancing the density of fibres in long-lived Twi mice suggests that BM-derived cells are major contributors in the attempt of correcting PNS disease.

An important indication of functional rescue provided by combined treatments came from the neurophysiological evaluation. The MCV, cMAP amplitude and CCT are deteriorated and often not measurable in end-stage Twi mice, due to compromised PNS and CNS. In strike contrast, all neurophysiological parameters were stabilized (although not rescued to physiological levels) in long-lived combined-treated Twi mice. In particular, cMAP amplitude and MCV showed a moderate but stable improvement that closely correlates with the number and density of myelinated fibres underscored by the morphometric analysis. We believe that these data provide proof-of-concept of efficacy of the proposed combined treatments in preserving PNS and CNS functionality in Twi mice.

In addition to demyelination, neuronal defects have occasionally been described in GLD patients (62,63). In the Twitcher mouse, early neuronal dysfunction occurs before demyelination (64) and advances with disease progression, ultimately leading to neuronal death (34,65). We have previously shown a link between *atf3* upregulation in Twi SC tissues and disease progression (35). We show here the specific upregulation of ATF3 expression in SC motor neurons, a population that appears particularly vulnerable to early cell distress (66,67). Even if the role of ATF3 upregulation in damaged neurons is not completely understood (37,68), the rapid and stable downregulation to physiological levels observed in combined-treated Twi mice suggests an additional benefit provided by this treatment. Notably, we showed upregulation of *hATF3* mRNA expression in CNS tissues of GLD patients, suggesting a possible involvement of neuronal stress in the human pathogenesis.

We have proven a unique therapeutic advantage of combined treatments over individual ones, primarily due to their ability to deliver appropriate enzymatic supply at all relevant disease sites at due time. In particular, the early contribution provided by NSCT and IC GT appears critically relevant to counterbalance the onset/progression of CNS pathology. This short-term advantage is decisive to ensure enhanced long-term benefit upon BMT. Eventually, astrogliosis and myelin dysfunction result the most refractory disease-associated hallmarks to be corrected. In particular, the apparent resiliency of PNS to functional rescue, despite the good enzymatic reconstitution, implies a fundamental role of CNS correction to achieve outstanding therapeutic benefit in this disease model, which was not acknowledged previously. Also, the extent of tissue damage that is present at the time in which therapies start to be effective is critical for the therapeutic outcome. In this perspective, treatment performed in the early asymptomatic stages and the use of gene-corrected, GALC overexpressing HSCs (instead of BM-derived HCs expressing physiological GALC activity) in this setting (11,32,69) may further improve the overall therapeutic potential of the combined approach and result in effective correction of most disease-related abnormalities. Indeed, HSC GT exploiting autologous genetically modified HSCs has been shown to significantly halt progression in presymptomatic children with late infantile MLD (70), a related LSD for which allogeneic HSCT failed to prove unambiguous benefit.

In conclusion, the combination of the cell/gene therapy protocols proposed here, which are in advanced stage of clinical development as individual treatments for several neurodegenerative/demyelinating disorders (41,44,71), may constitute a feasible and potentially effective treatment opportunity for children affected by the severe GLD forms and, possibly, similar LSDs.

Materials and Methods

Mice

Twitcher mice bear a spontaneous point mutation resulting in a premature stop codon and no residual GALC activity (72). In this

study, we used galc–/– mice on the mixed background of C57BL/6 and FVB, generated by breeding C57BL/6 Twitcher heterozygous (galc+/–) mice with WT (galc+/+) FVB mice (Jackson Laboratory, Bar Harbor, ME, USA). FVB/Twitcher (–/–) (referred to as *Twi mice* in this study) have been previously described (5,29,73).

GFP transgenic mice (TgGFP) on the FVB background were generated by means of LV-mediated transgenesis using a phosphoglycerate kinase (PGK) promoter. GFP construct as previously described (74). Animals characterized by integration of two LV copies were used as BM donors. GALC transgenic Twi mice (TgGALC Twi) were first generated by the same protocol used to generate Arylsulfatase A transgenic mice (75), with a LV carrying the mGALC cDNA under the control of the PGK promoter in the FVB background. Animals were then crossed with Twitcher mice (C57BL/6) to achieve *galc–/–* mixed background and those characterized by integration of 2, 4 and 6 LV copies were used for GALC assay. Mouse colonies were maintained in the animal facility of the San Raffaele Scientific Institute, Milano, Italy. All experiments and procedures described in this study were conducted under an approved protocol of the 'Institutional Committee for the Good Animal Experimentation' of the San Raffaele Scientific Institute and are reported to the Ministry of Health, as required by Italian law.

Lentiviral vectors

We used monocistronic and bidirectional (bd) self-inactivating-LVs, the latter allowing the coordinate expression of two transgenes driven by the human PGK promoter (76). For *NSC transduction* we used a bdLV expressing the murine GALC and the enhanced (e)GFP genes (bdLV.GALC) (29). Titer of concentrated vector was 1×10^9 TU/ml. For *IC GT* we used monocistronic LVs expressing hGALC (LV.hGALC) or the GFP cDNAs (LV.GFP) under the control of the PGK promoter. Titers of concentrated vectors were 3.8×10^9 TU/ml and 1.45×10^9 TU/ml, respectively. All the procedures relative to LV preparation and titration have been previously described (40,76,77). The overlapping biodistribution and transgene expression of monocistronic and bidirectional LVs upon *in vitro* and *in vivo* transduction has been previously demonstrated (5,29).

Generation of LV-transduced NSC lines

Gene-corrected NSC lines ($n = 2$) to be used for transplantation experiments were established as previously described (77,78). We evaluated the efficacy of bdLV transduction by quantifying: (i) the number of GFP expressing cells by fluorescence-activated cell sorting (FACS) analyses (96.2–100%); (ii) the vector copy number (VCN) by qPCR (16–17 copies/genome); (iii) GALC activity by a specific biochemical assay (79) (190 ± 25 nmol/h∗mg; mean ± SEM, $n = 4$, two independent replicates for each gene-corrected NSC line; GALC activity in the parental, untransduced NSC lines was 49.74 ± 15.35 nmol/h∗mg; mean ± SEM, $n = 4$).

Treatments

Intracerebral gene therapy (IC GT)

Post-natal day (PND)2 Twi mice were anaesthetized in crushed ice and placed on a refrigerated stage. The therapeutic or control vectors (2×10^6 TU/1 μl) were injected unilaterally in the EC under stereotactic guidance using a glass capillary mounted on a micromanipulator (5). Stereotactic coordinates (mm from the frontal cerebral vein): AP +1, ML +2, DV –1.

Neural stem cell transplant (NSCT)

Serially passaged gene-corrected NSCs were mechanically dissociated 48 h before the transplantation. Just prior to transplantation cells were collected, centrifuged, mildly dissociated, counted and suspended in PBS + 0.1% DNase (Sigma). NSCs were delivered bilaterally in the lateral ventricles of PND2 mice (2.5×10^5 cells/1 μl/hemisphere) through a glass capillary (29).

Bone marrow transplant

Total BM was flushed from tibias, femurs and humeri of 4- to 8-week-old WTtgGFP mice using PBS + 2% FBS and then centrifuged at 800*g* for 5 min. After lysis in ddH_2O the cell suspension was flowed through a 40 μm cell strainer (BD Biosciences). One WTtgGFP mouse could serve as donor for six recipient mice. Cells are suspended in PBS and immediately injected in the jugular vein of lethally irradiated PND7 Twi and WT mice (5×10^6 cells/30 μl). The survival after the procedure was ∼70%.

Part of the BM suspension was collected and analyzed for GFP expression (by FACS analysis) and GALC activity. About 72% of BM cells isolated from tgGFP mice expressed GFP. TgGFP BM cells expressed physiological levels of GALC activity (23.02 ± 0.5 nmol/h∗mg; $n = 3$).

Combined treatments

NSCT and IC GT were performed at PND2. Treated mice underwent myeloablation by total body irradiation at PND6 and BMT on the following day.

Mice dying within 2–3 weeks after irradiation were excluded from subsequent analyses. Mice were randomly assigned to treatment groups (cages, day of transplant, mice of the same cage sacrificed at different time points). The outcome of treatments was evaluated by several readouts (kinetics of cell engraftment, GALC reconstitution, markers of pathology, neurophysiology) applying extensive morphological, immunohistochemical, biochemical, molecular and functional analyses performed in a time-course modality on several affected tissues (CNS and periphery). In all the experiments, mice treated with the single approaches served as controls for the combined procedures. Two independent operators performed analysis of data blinded to experimental group.

Tissue collection and processing

Mice were deeply anesthetized with Avertine and intracardially perfused with 0.9% NaCl. Tissues to be used for biochemical and molecular assays (brain, SC, SN, liver and BM) were isolated and quickly frozen in liquid nitrogen.

A group of mice were perfused with 0.9% NaCl followed by 4% PFA. Brains and SC tissues were collected and equilibrated for 24 h in PFA and then included in 4% agarose. Serial coronal vibratome-cut sections (six series, 40 μm thick) were processed for IHC and immunofluorescence (IF) analyses as described below.

One SN of each animal was collected, equilibrated 24 h in 4% PFA, followed by successive 24 h incubation in 20% and 30% sucrose in PBS. After embedding in Tissue-Tek O.C.T. compound (Sakura, Torrance, CA, USA) and deep-freezing on dry ice, tissue was cut in transverse sections (14 μm) in a cryostat (Leica, Heidelberg, Germany) and mounted onto SuperFrost slides. For morphometric analyses, SNs were collected, equilibrated in 2% glutaraldehyde and included for microtome processing.

Human tissues

Post-mortem snap-frozen brain samples from GLD patients and normal donors (ND) were obtained from the National Institute of Child Health and Human Development Brain and Tissue Bank for Developmental Disorders at University of Maryland, Baltimore.

FACS analysis to determine HC engraftment

BM and PB samples from BMT and combined-treated Twi and WT mice were suspended in blocking solution (PBS + 5% FBS + 1% BSA) for 15 min and then rat anti-mouse CD45-PE (BD Pharmingen 553081) was added for 20 min. After washing in PBS, pellets were suspended in 300 μl of PBS. Cells were analyzed for CD45 and GFP positivity using a flow cytometer (Canto II, BD Biosciences). Data were analyzed using the FlowJo software.

IHC and IF assays

Vibratome-cut sections and cryostat sections were processed for IHC, IF analyses and lectin histochemistry, following previously described protocols (29,35,50). A list of antibodies used can be found in Supplementary Material, Table S1.

Quantification of engrafted cells

We analyzed matched coronal brain and SC sections using anti-GFP antibody in combination with lineage-specific markers (NeuN and PSA-NCAM, for neurons; GFAP, for astroglia; APC and MBP, for oligodendroglia; CD45 and Iba1 for HCs and microglia, respectively), markers of apoptosis (C3), proliferation (Ki67) and cellular stress (ATF3) and nuclear counterstaining (ToPro-3) in IF analysis followed by confocal microscopy analysis. Results were expressed as: (i) the percentage of GFP^+ NSCs on the total number of transplanted cells (engraftment); GFP^+ NSCs were counted in coronal brain sections (15–18 sections/mice, one out of six series). This number was multiplied by six, in order to have an estimate of the total number of engrafted cells/brain; (ii) the percentage of $PSA\text{-}NCAM^+$, $GFAP^+$ or APC^+ cells within the GFP^+ NSC population or the LV.GFP-transduced cells (we counted 1000–2000 GFP^+ cells, two slices/mouse, $n = 3$–6 mice); (iii) the percentage of $C3^+$ cells and $ATF3^+$ neurons (we counted a total number of 1970 $C3^+$ cells and 13 603 $NeuN^+$ cells in 2–4 slices/mouse, $n = 3$–10 mice); (iv) the percentage of $Ki67^+$ or $C3^+$ cells within the GFP^+ microglial cells (we counted a total number of 600 $Ki67^+$ cells on a total of 904 GFP^+ myeloid cells, 6 slices/mouse, $n = 3$ mice).

Images were acquired with Zeiss Axioskop2 microscope using double laser confocal microscopy with Zeiss Plan-Neofluar objective lens (Zeiss, Arese, Italy), Radiance 2100 camera (Bio-Rad, Segrate, Italy) and LaserSharp 2000 acquisition software (Bio-Rad); PerkinElmer UltraVIEW ERS Spinning Disk Confocal (PerkinElmer Life Sciences, Inc., MA, USA). Images are imported into Adobe Photoshop CS4 (USA) and adjusted for brightness and contrast.

Quantification of immunopositive area

Slices processed for IHC (lectin and GFAP) were visualized with a Nikon Eclipse E600 microscope. Images were acquired at 10× magnification in bright field using a Nikon DMX 1200 digital camera and ACT-1 acquisition software (Nikon). Pictures of matched areas in each slice (selected as described previously) (29) were taken and the immunopositive area in each picture (expressed in pixels) was calculated using the ImageJ software. Tissue slices from UT WT mice were used to set the signal threshold.

Determination of GALC activity

GALC activity in tissues and cells was measured as previously described (5,29,79).

Psychosine measurement

Psychosine dosage was performed in frozen tissues by TSQ Quantum AM mass spectrometer (Thermo) as previously described (5).

Gene expression analyses

Total RNA from murine and human CNS tissues was extracted according to the manufacturer protocol of RNeasy Lipid Tissue with Qiazol (Qiagen). The quantity of RNA was determined by 260/280 nm optical density (OD) reading on a NanoDrop ND-1000 Spectrophotometer (NanoDrop, Pero, Italy). mRNA reverse transcription (RT) was performed according to the manufacturer protocol of QuantiTect reverse transcription kit (Qiagen). Quantitative PCR (qPCR) was performed in Optical 96-well Fast Thermal Cycling Plates (Applied Biosystems) on ABI PRISM 7900 Sequence Detector System (Applied Biosystems) or Viia7 (Applied Biosystems), using the following thermal cycling conditions: for SYBR green qPCR one cycle at 95°C for 5 min, 40 cycles at 95°C for 10 s and 60°C for 30 s; for TaqMan qPCR one cycle at 95°C for 5 min, 40 cycle at 95°C for 15 s and 60°C for 1 min. Each sample is run in duplicate in a total volume of 25 μl/reaction, containing 12.5 μl 2× QuantiFast SYBR Green PCR Master Mix, 2 μl of template cDNA and 2.5 μl QuantiTect Primer Assays (all from Qiagen) or containing 12.5 μl 2× Universal PCR Master Mix (Applied Biosystems), 2 μl of template cDNA and 1.25 μl of Probe + Primers (TaqMan Gene Expression Assays, Applied Biosystems). Commercial probes and primers used are reported in Supplementary Material, Table S2. The SDS 2.2.1 software was used to extract raw data. Relative expression of mRNA for the target genes was performed by the comparative CT (ΔΔCT) method using selected housekeeping genes as control. The relative mRNA levels were expressed as fold change over WT (mouse) or ND (human). Statistical analyses were performed on ΔΔCT values.

Morphometric analysis on SNs

Semi thin section analysis of SNs was performed as reported (80). The total number of myelinated axons and their density (ratio between the number of fibres and the area per mm^2) was calculated by counting all fibres in an entire reconstructed nerve section. The number of axons plotted for the axonal diameter was calculated using five images of a nerve section randomly acquired.

Neurophysiological evaluation

The motor MCV, the cMAP and the CCT (measured as the difference between cortical motor evoked potentials and peripheral conduction time latencies) were measured as reported (32). Of note, CCT was not reliably measurable in 80% of UT and treated Twi mice. This was not totally unexpected, since CCT is indirectly derived and depends on the presence of cMAPs, a parameter that is altered in Twi mice due to the dysfunctional PNS.

Statistics

The results were analyzed with Graph Pad Prism version 5.0a for Macintosh. Unpaired Student's *t*-test, One- or Two-way ANOVA or non-parametric tests followed by appropriate post-tests were used according to the datasets to be analyzed (statistical significance: $P < 0.05$). Survival curves were analyzed by Log-Rank (Mantel–Cox) test. The sample size and the statistical tests used are described in the figure legends.

Authors' Contributions

A.G., A.R. and N.R. were primarily responsible for experimental design, data analysis and writing of this paper. A.B. contributed to experimental design, interpretation of data and manuscript revision. S.U. was responsible for BMT experiments. S.M. and F.M. were responsible for GALC analysis. W.K. was responsible for Psy analysis. F.B. and U.D.C. were responsible for neurophysiological assessment. V.A. and A.Bo. were responsible for morphometric analysis on PNS tissues.

Supplementary Material

Supplementary Material is available at *HMG* online.

Acknowledgments

We thank A. Montepeloso for help with BM transplant; A. Lattanzi and C. Salvagno for help with IC GT; H. van Lenthe for sample preparation and analysis of Psy; L. Rampoldi and C. Schaeffer for providing anti-ATF3 antibody; all the people in A. Gritti's team for constant support; L. Naldini and V. Broccoli for helpful discussion.

Conflict of Interest statement. None declared.

Funding

This work was supported by: Comitato Telethon Fondazione Onlus, grants numbers TGT11B02 (to A.G.), TGT11B01 (to A.B.), GPP10007D and GGP12017 (to A.Bo.); the EU Seventh Framework Program (FP7)-HEALTH-F2-2010-241622 (Therapeutic Challenge in Leukodystrophies, LEUKOTREAT) and the National Tay-Sachs & Allied Diseases association (NTSAD2008) to A.B. and A.G.; Association Française contre les Myopathies (AFM)-France (grant no. 16040/16922) and the E-Rare JTC2011 (to A.Bo.). Funding to pay the Open Access publication charges for this article was provided by Fondazione Telethon, Via Varese 16b – 00185 Rome, Italy.

References

1. Suzuki, K. (2003) Globoid cell leukodystrophy (Krabbe's disease): update. *J. Child Neurol.*, **18**, 595–603.
2. LeVine, S.M., Pedchenko, T.V., Bronshteyn, I.G. and Pinson, D.M. (2000) L-cycloserine slows the clinical and pathological course in mice with globoid cell leukodystrophy (twitcher mice). *J. Neurosci. Res.*, **60**, 231–236.
3. Lee, W.C., Tsoi, Y.K., Troendle, F.J., DeLucia, M.W., Ahmed, Z., Dicky, C.A., Dickson, D.W. and Eckman, C.B. (2007) Single-dose intracerebroventricular administration of galactocerebrosidase improves survival in a mouse model of globoid cell leukodystrophy. *FASEB J.*, **21**, 2520–2527.
4. Lin, D.S., Hsiao, C.D., Liau, I., Lin, S.P., Chiang, M.F., Chuang, C.K., Wang, T.J., Wu, T.Y., Jian, Y.R., Huang, S.F. *et al.* (2011) CNS-targeted AAV5 gene transfer results in global dispersal of vector and prevention of morphological and function deterioration in CNS of globoid cell leukodystrophy mouse model. *Mol. Genet. Metab.*, **103**, 367–377.
5. Lattanzi, A., Salvagno, C., Maderna, C., Benedicenti, F., Morena, F., Kulik, W., Naldini, L., Montini, E., Martino, S. and Gritti, A. (2014) Therapeutic benefit of lentiviral-mediated neonatal intracerebral gene therapy in a mouse model of globoid cell leukodystrophy. *Hum. Mol. Genet.*, **23**, 3250–3268.
6. Suzuki, K., Hoogerbrugge, P.M., Poorthuis, B.J. and Bekkum, D.W. (1988) The twitcher mouse. Central nervous system pathology after bone marrow transplantation. *Lab. Invest.*, **58**, 302–309.
7. Hoogerbrugge, P.M., Suzuki, K., Poorthuis, B.J., Kobayashi, T., Wagemaker, G. and van Bekkum, D.W. (1988) Donor-derived cells in the central nervous system of twitcher mice after bone marrow transplantation. *Science*, **239**, 1035–1038.
8. Yagi, T., Matsuda, J., Tominaga, K. and Suzuki, K. (2005) Hematopoietic cell transplantation ameliorates clinical phenotype and progression of the CNS pathology in the mouse model of late onset Krabbe disease. *J. Neuropathol. Exp. Neurol.*, **64**, 565–575.
9. Yeager, A.M., Brennan, S., Tiffany, C., Moser, H.W. and Santos, G.W. (1984) Prolonged survival and remyelination after hematopoietic cell transplantation in the twitcher mouse. *Science*, **225**, 1052–1054.
10. Luzi, P., Rafi, M.A., Zaka, M., Rao, H.Z., Curtis, M., Vanier, M.T. and Wenger, D.A. (2005) Biochemical and pathological evaluation of long-lived mice with globoid cell leukodystrophy after bone marrow transplantation. *Mol. Genet. Metab.*, **86**, 150–159.
11. Gentner, B., Visigalli, I., Hiramatsu, H., Lechman, E., Ungari, S., Giustacchini, A., Schira, G., Amendola, M., Quattrini, A., Martino, S. *et al.* (2010) Identification of hematopoietic stem cell-specific miRNAs enables gene therapy of globoid cell leukodystrophy. *Sci. Transl. Med.*, **2**, 58ra84.
12. Taylor, R.M., Lee, J.P., Palacino, J.J., Bower, K.A., Li, J., Vanier, M.T., Wenger, D.A., Sidman, R.L. and Snyder, E.Y. (2006) Intrinsic resistance of neural stem cells to toxic metabolites may make them well suited for cell non-autonomous disorders: evidence from a mouse model of Krabbe leukodystrophy. *J. Neurochem.*, **97**, 1585–1599.
13. Pellegatta, S., Tunici, P., Poliani, P.L., Dolcetta, D., Cajola, L., Colombelli, C., Ciusani, E., Di Donato, S. and Finocchiaro, G. (2006) The therapeutic potential of neural stem/progenitor cells in murine globoid cell leukodystrophy is conditioned by macrophage/microglia activation. *Neurobiol. Dis.*, **21**, 314–323.
14. Ripoll, C.B., Flaat, M., Klopf-Eiermann, J., Fisher-Perkins, J.M., Trygg, C.B., Scruggs, B.A., McCants, M.L., Leonard, H.P., Lin, A.F., Zhang, S. *et al.* (2010) Mesenchymal-lineage stem cells have pronounced anti-inflammatory effects in the twitcher mouse model of Krabbe's disease. *Stem Cells*, **29**, 67–77.
15. Scruggs, B.A., Zhang, X., Bowles, A.C., Gold, P.A., Semon, J.A., Fisher-Perkins, J.M., Zhang, S., Bonvillain, R.W., Myers, L., Chen Li, S. *et al.* (2013) Multipotent Stromal cells alleviate inflammation, neuropathology, and symptoms associated with globoid cell leukodystrophy in the twitcher mouse. *Stem Cells*, **31**, 1523–1534.
16. Miranda, C.O., Teixeira, C.A., Liz, M.A., Sousa, V.F., Franquinho, F., Forte, G., Di Nardo, P., Pinto-Do, O.P. and Sousa, M.M. (2011) Systemic delivery of bone marrow-derived mesenchymal stromal cells diminishes neuropathology in a mouse model of Krabbe's disease. *Stem Cells*, **29**, 1738–1751.
17. Krivit, W., Sung, J.H., Shapiro, E.G. and Lockman, L.A. (1995) Microglia: the effector cell for reconstitution of the central

nervous system following bone marrow transplantation for lysosomal and peroxisomal storage diseases. *Cell Transplant.*, **4**, 385–392.
18. Biffi, A., Aubourg, P. and Cartier, N. (2011) Gene therapy for leukodystrophies. *Hum. Mol. Genet.*, **20**, R42–R53.
19. Boelens, J.J. (2006) Trends in haematopoietic cell transplantation for inborn errors of metabolism. *J. Inherit. Metab. Dis.*, **29**, 413–420.
20. Escolar, M.L., Poe, M.D., Provenzale, J.M., Richards, K.C., Allison, J., Wood, S., Wenger, D.A., Pietryga, D., Wall, D., Champagne, M. *et al.* (2005) Transplantation of umbilical-cord blood in babies with infantile Krabbe's disease. *N. Engl. J. Med.*, **352**, 2069–2081.
21. Duffner, P.K., Caviness, V.S. Jr., Erbe, R.W., Patterson, M.C., Schultz, K.R., Wenger, D.A. and Whitley, C. (2009) The long-term outcomes of presymptomatic infants transplanted for Krabbe disease: report of the workshop held on July 11 and 12, 2008, Holiday Valley, New York. *Genet. Med.*, **11**, 450–454.
22. Biswas, S. and LeVine, S.M. (2002) Substrate-reduction therapy enhances the benefits of bone marrow transplantation in young mice with globoid cell leukodystrophy. *Pediatr. Res.*, **51**, 40–47.
23. Qin, E.Y., Hawkins-Salsbury, J.A., Jiang, X., Reddy, A.S., Farber, N.B., Ory, D.S. and Sands, M.S. (2012) Bone marrow transplantation increases efficacy of central nervous system-directed enzyme replacement therapy in the murine model of globoid cell leukodystrophy. *Mol. Genet. Metab.*, **107**, 186–196.
24. Lin, D., Donsante, A., Macauley, S., Levy, B., Vogler, C. and Sands, M.S. (2007) Central nervous system-directed AAV2/5-mediated gene therapy synergizes with bone marrow transplantation in the murine model of globoid-cell leukodystrophy. *Mol. Ther.*, **15**, 44–52.
25. Reddy, A.S., Kim, J.H., Hawkins-Salsbury, J.A., Macauley, S.L., Tracy, E.T., Vogler, C.A., Han, X., Song, S.K., Wozniak, D.F., Fowler, S.C. *et al.* (2011) Bone marrow transplantation augments the effect of brain- and spinal cord-directed adeno-associated virus 2/5 gene therapy by altering inflammation in the murine model of globoid-cell leukodystrophy. *J. Neurosci.*, **31**, 9945–9957.
26. Galbiati, F., Givogri, M.I., Cantuti, L., Rosas, A.L., Cao, H., van Breemen, R. and Bongarzone, E.R. (2009) Combined hematopoietic and lentiviral gene-transfer therapies in newborn Twitcher mice reveal contemporaneous neurodegeneration and demyelination in Krabbe disease. *J. Neurosci. Res.*, **87**, 1748–1759.
27. Reddy, A.S., Wozniak, D.F., Farber, N.B., Dearborn, J.T., Fowler, S.C. and Sands, M.S. (2012) Bone marrow transplantation alters the tremor phenotype in the murine model of globoid-cell leukodystrophy. *J. Clin. Med.*, **1**, 1–14.
28. Rafi, M.A., Rao, H.Z., Luzi, P., Curtis, M.T. and Wenger, D.A. (2012) Extended normal life after AAVrh10-mediated gene therapy in the mouse model of Krabbe disease. *Mol. Ther.*, **20**, 2031–2042.
29. Neri, M., Ricca, A., di Girolamo, I., Alcala'-Franco, B., Cavazzin, C., Orlacchio, A., Martino, S., Naldini, L. and Gritti, A. (2011) Neural stem cell gene therapy ameliorates pathology and function in a mouse model of globoid cell leukodystrophy. *Stem Cells*, **29**, 1559–1571.
30. Pluchino, S., Quattrini, A., Brambilla, E., Gritti, A., Salani, G., Dina, G., Galli, R., Del Carro, U., Amadio, S., Bergami, A. *et al.* (2003) Injection of adult neurospheres induces recovery in a chronic model of multiple sclerosis. *Nature*, **422**, 688–694.
31. Biffi, A., Capotondo, A., Fasano, S., del Carro, U., Marchesini, S., Azuma, H., Malaguti, M.C., Amadio, S., Brambilla, R., Grompe, M. *et al.* (2006) Gene therapy of metachromatic leukodystrophy reverses neurological damage and deficits in mice. *J. Clin. Invest.*, **116**, 3070–3082.
32. Biffi, A., De Palma, M., Quattrini, A., Del Carro, U., Amadio, S., Visigalli, I., Sessa, M., Fasano, S., Brambilla, R., Marchesini, S. *et al.* (2004) Correction of metachromatic leukodystrophy in the mouse model by transplantation of genetically modified hematopoietic stem cells. *J. Clin. Invest.*, **113**, 1118–1129.
33. Alroy, J., Ucci, A.A., Goyal, V. and Woods, W. (1986) Lectin histochemistry of glycolipid storage diseases on frozen and paraffin-embedded tissue sections. *J. Histochem. Cytochem.*, **34**, 501–505.
34. Castelvetri, L.C., Givogri, M.I., Zhu, H., Smith, B., Lopez-Rosas, A., Qiu, X., van Breemen, R. and Bongarzone, E.R. (2011) Axonopathy is a compounding factor in the pathogenesis of Krabbe disease. *Acta Neuropathol.*, **122**, 35–48.
35. Meisingset, T.W., Ricca, A., Neri, M., Sonnewald, U. and Gritti, A. (2013) Region- and age-dependent alterations of glial-neuronal metabolic interactions correlate with CNS pathology in a mouse model of globoid cell leukodystrophy. *J. Cereb. Blood Flow Metab.*, **33**, 1127–1137.
36. Cachon-Gonzalez, M.B., Wang, S.Z., Ziegler, R., Cheng, S.H. and Cox, T.M. (2014) Reversibility of neuropathology in Tay-Sachs-related diseases. *Hum. Mol. Genet.*, **23**, 730–748.
37. Hunt, D., Raivich, G. and Anderson, P.N. (2012) Activating transcription factor 3 and the nervous system. *Front. Mol. Neurosci.*, **5**, 7.
38. Dolcetta, D., Amadio, S., Guerrini, U., Givogri, M.I., Perani, L., Galbiati, F., Sironi, L., Del Carro, U., Roncarolo, M.G. and Bongarzone, E. (2005) Myelin deterioration in Twitcher mice: motor evoked potentials and magnetic resonance imaging as in vivo monitoring tools. *J. Neurosci. Res.*, **81**, 597–604.
39. Smith, B., Galbiati, F., Castelvetri, L.C., Givogri, M.I., Lopez-Rosas, A. and Bongarzone, E.R. (2011) Peripheral neuropathy in the Twitcher mouse involves the activation of axonal caspase 3. *ASN Neuro*, **3**, pii: e000066.
40. Visigalli, I., Moresco, R.M., Belloli, S., Politi, L.S., Gritti, A., Ungaro, D., Matarrese, M., Turolla, E., Falini, A., Scotti, G. *et al.* (2009) Monitoring disease evolution and treatment response in lysosomal disorders by the peripheral benzodiazepine receptor ligand PK11195. *Neurobiol. Dis.*, **34**, 51–62.
41. Selden, N.R., Al-Uzri, A., Huhn, S.L., Koch, T.K., Sikora, D.M., Nguyen-Driver, M.D., Guillaume, D.J., Koh, J.L., Gultekin, S.H., Anderson, J.C. *et al.* (2013) Central nervous system stem cell transplantation for children with neuronal ceroid lipofuscinosis. *J. Neurosurg. Pediatr.*, **11**, 643–652.
42. Worgall, S., Sondhi, D., Hackett, N.R., Kosofsky, B., Kekatpure, M.V., Neyzi, N., Dyke, J.P., Ballon, D., Heier, L., Greenwald, B.M. *et al.* (2008) Treatment of late infantile neuronal ceroid lipofuscinosis by CNS administration of a serotype 2 adeno-associated virus expressing CLN2 cDNA. *Hum. Gene Ther.*, **19**, 463–474.
43. Tardieu, M., Zerah, M., Husson, B., de Bournonville, S., Deiva, K., Adamsbaum, C., Vincent, F., Hocquemiller, M., Broissand, C., Furlan, V. *et al.* (2014) Intracerebral administration of AAV rh.10 carrying human SGSH and SUMF1 cDNAs in children with MPSIIIA disease: results of a phase I/II trial. *Hum. Gene Ther.*, **25**, 506–516.
44. Palfi, S., Gurruchaga, J.M., Ralph, G.S., Lepetit, H., Lavisse, S., Buttery, P.C., Watts, C., Miskin, J., Kelleher, M., Deeley, S. *et al.* (2014) Long-term safety and tolerability of ProSavin, a lentiviral vector-based gene therapy for Parkinson's disease: a dose escalation, open-label, phase 1/2 trial. *Lancet*, **383**, 1138–1146.

45. Mingozzi, F. and High, K.A. (2013) Immune responses to AAV vectors: overcoming barriers to successful gene therapy. *Blood*, **122**, 23–36.
46. Lee, J.P., Jeyakumar, M., Gonzalez, R., Takahashi, H., Lee, P.J., Baek, R.C., Clark, D., Rose, H., Fu, G., Clarke, J. *et al.* (2007) Stem cells act through multiple mechanisms to benefit mice with neurodegenerative metabolic disease. *Nat. Med.*, **13**, 439–447.
47. Pluchino, S., Zanotti, L., Rossi, B., Brambilla, E., Ottoboni, L., Salani, G., Martinello, M., Cattalini, A., Bergami, A., Furlan, R. *et al.* (2005) Neurosphere-derived multipotent precursors promote neuroprotection by an immunomodulatory mechanism. *Nature*, **436**, 266–271.
48. Tamaki, S.J., Jacobs, Y., Dohse, M., Capela, A., Cooper, J.D., Reitsma, M., He, D., Tushinski, R., Belichenko, P.V., Salehi, A. *et al.* (2009) Neuroprotection of host cells by human central nervous system stem cells in a mouse model of infantile neuronal ceroid lipofuscinosis. *Cell Stem Cell*, **5**, 310–319.
49. Cossetti, C., Iraci, N., Mercer, T.R., Leonardi, T., Alpi, E., Drago, D., Alfaro-Cervello, C., Saini, H.K., Davis, M.P., Schaeffer, J. *et al.* (2014) Extracellular vesicles from neural stem cells transfer IFN-gamma via Ifngr1 to activate Stat1 signaling in target cells. *Mol. Cell*, **56**, 193–204.
50. Santambrogio, S., Ricca, A., Maderna, C., Ieraci, A., Aureli, M., Sonnino, S., Kulik, W., Aimar, P., Bonfanti, L., Martino, S. *et al.* (2012) The galactocerebrosidase enzyme contributes to maintain a functional neurogenic niche during early post-natal CNS development. *Hum. Mol. Genet.*, **21**, 4732–4750.
51. McGraw, P., Liang, L., Escolar, M., Mukundan, S., Kurtzberg, J. and Provenzale, J.M. (2005) Krabbe disease treated with hematopoietic stem cell transplantation: serial assessment of anisotropy measurements—initial experience. *Radiology*, **236**, 221–230.
52. Escolar, M.L., Poe, M.D., Smith, J.K., Gilmore, J.H., Kurtzberg, J., Lin, W. and Styner, M. (2009) Diffusion tensor imaging detects abnormalities in the corticospinal tracts of neonates with infantile Krabbe disease. *AJNR Am. J. Neuroradiol.*, **30**, 1017–1021.
53. Galbiati, F., Basso, V., Cantuti, L., Givogri, M.I., Lopez-Rosas, A., Perez, N., Vasu, C., Cao, H., van Breemen, R., Mondino, A. *et al.* (2007) Autonomic denervation of lymphoid organs leads to epigenetic immune atrophy in a mouse model of Krabbe disease. *J. Neurosci.*, **27**, 13730–13738.
54. Varvel, N.H., Grathwohl, S.A., Baumann, F., Liebig, C., Bosch, A., Brawek, B., Thal, D.R., Charo, I.F., Heppner, F.L., Aguzzi, A. *et al.* (2012) Microglial repopulation model reveals a robust homeostatic process for replacing CNS myeloid cells. *Proc. Natl. Acad. Sci. U. S. A.*, **109**, 18150–18155.
55. Ajami, B., Bennett, J.L., Krieger, C., McNagny, K.M. and Rossi, F.M. (2011) Infiltrating monocytes trigger EAE progression, but do not contribute to the resident microglia pool. *Nat. Neurosci.*, **14**, 1142–1149.
56. Igisu, H. and Suzuki, K. (1984) Progressive accumulation of toxic metabolite in a genetic leukodystrophy. *Science*, **224**, 753–755.
57. Wu, Y.P., McMahon, E.J., Matsuda, J., Suzuki, K. and Matsushima, G.K. (2001) Expression of immune-related molecules is downregulated in twitcher mice following bone marrow transplantation. *J. Neuropathol. Exp. Neurol.*, **60**, 1062–1074.
58. Shechter, R., London, A., Varol, C., Raposo, C., Cusimano, M., Yovel, G., Rolls, A., Mack, M., Pluchino, S., Martino, G. *et al.* (2009) Infiltrating blood-derived macrophages are vital cells playing an anti-inflammatory role in recovery from spinal cord injury in mice. *PLoS Med.*, **6**, e1000113.
59. Siddiqi, Z.A., Sanders, D.B. and Massey, J.M. (2006) Peripheral neuropathy in Krabbe disease: electrodiagnostic findings. *Neurology*, **67**, 263–267.
60. Kondo, A., Hoogerbrugge, P.M., Suzuki, K., Poorthuis, B.J. and Van Bekkum, D.W. (1988) Pathology of the peripheral nerve in the twitcher mouse following bone marrow transplantation. *Brain Res*, **460**, 178–183.
61. Siddiqi, Z.A., Sanders, D.B. and Massey, J.M. (2006) Peripheral neuropathy in Krabbe disease: effect of hematopoietic stem cell transplantation. *Neurology*, **67**, 268–272.
62. Dunn, H.G., Lake, B.D., Dolman, C.L. and Wilson, J. (1969) The neuropathy of Krabbe's infantile cerebral sclerosis (globoid cell leucodystrophy). *Brain*, **92**, 329–344.
63. Itoh, M., Hayashi, M., Fujioka, Y., Nagashima, K., Morimatsu, Y. and Matsuyama, H. (2002) Immunohistological study of globoid cell leukodystrophy. *Brain Dev.*, **24**, 284–290.
64. Teixeira, C.A., Miranda, C.O., Sousa, V.F., Santos, T.E., Malheiro, A.R., Solomon, M., Maegawa, G.H., Brites, P. and Sousa, M.M. (2014) Early axonal loss accompanied by impaired endocytosis, abnormal axonal transport, and decreased microtubule stability occur in the model of Krabbe's disease. *Neurobiol. Dis.*, **66**, 92–103.
65. Cantuti-Castelvetri, L., Zhu, H., Givogri, M.I., Chidavaenzi, R.L., Lopez-Rosas, A. and Bongarzone, E.R. (2012) Psychosine induces the dephosphorylation of neurofilaments by deregulation of PP1 and PP2A phosphatases. *Neurobiol. Dis.*, **46**, 325–335.
66. Vlug, A.S., Teuling, E., Haasdijk, E.D., French, P., Hoogenraad, C.C. and Jaarsma, D. (2005) ATF3 expression precedes death of spinal motoneurons in amyotrophic lateral sclerosis-SOD1 transgenic mice and correlates with c-Jun phosphorylation, CHOP expression, somato-dendritic ubiquitination and Golgi fragmentation. *Eur. J. Neurosci.*, **22**, 1881–1894.
67. Malaspina, A., Ngoh, S.F., Ward, R.E., Hall, J.C., Tai, F.W., Yip, P. K., Jones, C., Jokic, N., Averill, S.A., Michael-Titus, A.T. *et al.* (2010) Activation transcription factor-3 activation and the development of spinal cord degeneration in a rat model of amyotrophic lateral sclerosis. *Neuroscience*, **169**, 812–827.
68. Zhang, S.J., Buchthal, B., Lau, D., Hayer, S., Dick, O., Schwaninger, M., Veltkamp, R., Zou, M., Weiss, U. and Bading, H. (2011) A signaling cascade of nuclear calcium-CREB-ATF3 activated by synaptic NMDA receptors defines a gene repression module that protects against extrasynaptic NMDA receptor-induced neuronal cell death and ischemic brain damage. *J. Neurosci.*, **31**, 4978–4990.
69. Visigalli, I., Delai, S., Politi, L.S., Di Domenico, C., Cerri, F., Mrak, E., D'Isa, R., Ungaro, D., Stok, M., Sanvito, F. *et al.* (2010) Gene therapy augments the efficacy of hematopoietic cell transplantation and fully corrects Mucopolysaccharidosis type I phenotype in the mouse model. *Blood*, **116**, 1857–1866.
70. Biffi, A., Montini, E., Lorioli, L., Cesani, M., Fumagalli, F., Plati, T., Baldoli, C., Martino, S., Calabria, A., Canale, S. *et al.* (2013) Lentiviral hematopoietic stem cell gene therapy benefits metachromatic leukodystrophy. *Science*, **341**, 1233158.
71. McGlynn, M. (2012) StemCells, Inc.: clinical trials of stem cell therapies for CNS disorders. *Regen. Med.*, **7**, 8–11.
72. Suzuki, K. (1995) The twitcher mouse: a model for Krabbe disease and for experimental therapies. *Brain Pathol.*, **5**, 249–258.
73. Meisingset, T.W., Risa, O., Brenner, M., Messing, A. and Sonnewald, U. (2010) Alteration of glial-neuronal metabolic interactions in a mouse model of Alexander disease. *Glia*, **58**, 1228–1234.

74. Brown, B.D., Venneri, M.A., Zingale, A., Sergi Sergi, L. and Naldini, L. (2006) Endogenous microRNA regulation suppresses transgene expression in hematopoietic lineages and enables stable gene transfer. *Nat. Med.*, **12**, 585–591.
75. Capotondo, A., Cesani, M., Pepe, S., Fasano, S., Gregori, S., Tononi, L., Venneri, M.A., Brambilla, R., Quattrini, A., Ballabio, A. *et al.* (2007) Safety of arylsulfatase A overexpression for gene therapy of metachromatic leukodystrophy. *Hum. Gene Ther.*, **18**, 821–836.
76. Amendola, M., Venneri, M.A., Biffi, A., Vigna, E. and Naldini, L. (2005) Coordinate dual-gene transgenesis by lentiviral vectors carrying synthetic bidirectional promoters. *Nat. Biotechnol.*, **23**, 108–116.
77. Neri, M., Maderna, C., Ferrari, D., Cavazzin, C., Vescovi, A.L. and Gritti, A. (2010) Robust generation of oligodendrocyte progenitors from human neural stem cells and engraftment in experimental demyelination models in mice. *PLoS ONE*, **5**, e10145.
78. Gritti, A., Dal Molin, M., Foroni, C. and Bonfanti, L. (2009) Effects of developmental age, brain region, and time in culture on long-term proliferation and multipotency of neural stem cell populations. *J. Comp. Neurol.*, **517**, 333–349.
79. Martino, S., Tiribuzi, R., Tortori, A., Conti, D., Visigalli, I., Lattanzi, A., Biffi, A., Gritti, A. and Orlacchio, A. (2009) Specific determination of beta-galactocerebrosidase activity via competitive inhibition of beta-galactosidase. *Clin. Chem.*, **55**, 541–548.
80. Wrabetz, L., Feltri, M.L., Quattrini, A., Imperiale, D., Previtali, S., D'Antonio, M., Martini, R., Yin, X., Trapp, B.D., Zhou, L. *et al.* (2000) P(0) glycoprotein overexpression causes congenital hypomyelination of peripheral nerves. *J. Cell Biol.*, **148**, 1021–1034.